Chapter 1
Amplitude Death, Synchrony, and Chimera States in Delay Coupled Limit Cycle Oscillators

Abhijit Sen, Ramana Dodla, George L. Johnston, and Gautam C. Sethia

1.1 Introduction

In this chapter we will discuss the effects of time delay on the collective states of a model mathematical system composed of a collection of coupled limit cycle oscillators. Such an assembly of coupled nonlinear oscillators serves as a useful paradigm for the study of collective phenomena in many physical, chemical, and biological systems and has therefore led to a great deal of theoretical and experimental work in the past [1–6]. Examples of practical applications of such models include simulating the interactions of arrays of Josephson junctions [7, 8], semiconductor lasers [9, 10], charge density waves [11], phase-locking of relativistic magnetrons [12], Belousov–Zhabotinskii reactions in coupled Brusselator models [2, 13–15], and neural oscillator networks for circadian pacemakers [16]. One of the most commonly studied phenomena is that of synchronization of the diverse frequencies of an oscillator assembly to a single common frequency. Synchrony was highlighted by Winfree [1] in a simple model of weakly coupled limit cycle oscillators and further developed by Kuramoto and others in the context of phase transition models [17, 18]. Research on synchrony in a variety of coupled and complex systems has seen an explosive growth in the past few years and has also captured the popular imagination [19] due to its application to such natural phenomena as the synchronous flashing of a swarm of fire flies, the chirping of crickets in unison, and the electrical synchrony in cardiac cells. Apart from synchrony, coupled limit cycle oscillator models are capable of exhibiting other interesting behavior. For example, if the strength of the interaction between the oscillators is comparable to the attraction to their own individual limit cycles, then the original phase-only model of Winfree or Kuramoto is no longer valid and the amplitudes of the individual oscillators begin to play a role [20–23]. For sufficiently strong coupling and a broad spread in the natural frequencies of the oscillators, the assembly can suffer an amplitude quenching or death [5, 24, 25] in which all the oscillators cease to oscillate and have zero amplitudes. Such

A. Sen (✉)
Institute for Plasma Research, Bhat, Gandhinagar 382428, India
e-mail: abhijit@ipr.res.in

F.M. Atay (ed.), *Complex Time-Delay Systems,* Understanding Complex Systems,
DOI 10.1007/978-3-642-02329-3_1,

behavior has been observed in experiments of coupled chemical oscillator systems, e.g., coupled Belousov–Zhabotinskii reactions carried out in coupled tank reactors [26]. Other collective phenomena that these coupled oscillator models display include partial synchronization, phase trapping, large amplitude Hopf oscillations, and even chaotic behavior [25, 27]—all of which have been discussed widely in the literature.

The question we wish to address now is what happens to the collective properties of the coupled oscillator system when one introduces time delay in the coupling. The physical motivation for such a modification of the coupling is to simulate the situation in real-life systems where the interaction between individual oscillators may not be instantaneous but may be delayed due to finite propagation time of signals. Time delays can similarly occur in chemical systems due to finite reaction times, and in biological systems like neuron assemblies, the synaptic integration mechanisms may provide a natural delay. From a mathematical point of view, one can expect time delays to have a profound effect on the dynamical characteristics of a single oscillator. This is well known from the study of single delay differential equations which show fundamental changes in the nature of solutions and novel effects that are absent in a non-delayed system. What happens to the collective modes of a coupled system in the presence of time delay? Surprisingly, there has not been a great deal of work in this area despite the vast literature on single delay differential equations and the considerable recent developments in the field of coupled oscillator research. Some notable exceptions are the works of Schuster and Wagner [28], Niebur et al. [29], Nakamura et al. [30], and Kim et al. [31], who in the past have looked at time delay effects in the context of the simple phase-only coupled oscillator models and found interesting effects like the existence of higher frequency states and changes in the onset conditions and nature of synchronization. More recently we have investigated a variety of model systems starting from a simple case of just two oscillators with a discrete time-delayed coupling to a large number of oscillators with time-delayed global, local, and non-local couplings [32–37]. Time delay is found to introduce significant changes in the character and onset properties of the various collective regimes such as amplitude death and phase-locked states. Some of the results are novel and somewhat surprising—such as time delay-induced death in an assembly of identical oscillators or the existence of clustered chimera states—and may have important applications. With a growing recognition of the significance and prevalence of time delay in various systems, there is now a considerable increase in the number of investigations on this topic. The aim of this chapter is to provide some appreciation of this interesting area of nonlinear dynamical systems through an exposition of the basic concepts of the field followed by a discussion of some research results. It is not meant to be a review of the field and the choices of topics and research results are heavily influenced by our own work.

The chapter is organized as follows. In Sect. 1.2 we develop the basics of the subject by introducing a minimal collective model consisting of two coupled limit cycle oscillators that are close to a supercritical Hopf bifurcation. After identifying the fundamental collective states of this system in the undelayed case we discuss the effects of a finite time delay on the existence and stability of phase-locked states

and amplitude death. In Sect. 1.3 we introduce a more complex model consisting of N-coupled oscillators ($N > 2$). The oscillators in such a system can be coupled in various ways: all-to-all (global), nearest neighbor (local), or spatially varying coupling (non-local). We discuss time-delayed collective states in all three systems and discuss their essential characteristics. Our primary emphasis is on the exploration of the *amplitude death state* in all three coupling scenarios. We also investigate the effect of time delay on a novel state of the non-local system—the so-called *chimera* state—consisting of co-existing regions of coherent and incoherent states. Time delay is seen to impose a spatial modulation of such a state leading to a *clustered chimera* state. Section 1.4 provides a summary of the main results and some perspective on the future directions and potential developments of the field.

1.2 A Minimal Collective Model

We begin our exploration of time delay effects on the collective states of coupled oscillator systems by investigating the dynamics of a minimal model system consisting of just two coupled limit cycle oscillators that are close to a supercritical Hopf bifurcation. The individual oscillator of this model is chosen to have the nonlinear normal form of a van der Pol-type equation. The van der Pol equation has a parameter that can be varied to take the solution state from a fixed point (a steady state) to an oscillatory state via a supercritical Hopf bifurcation. To illustrate this, consider the van der Pol equation in the following form:

$$\ddot{x} - (a - x^2)\dot{x} + \omega^2 x = 0. \tag{1.1}$$

In this and other equations below, the variables x, y, z, ξ, ϕ, ρ, and θ are functions of time, though, for simplicity, such a dependence is not explicitly written down, and a and ω are real parameters. For $a < 0$, $x = 0$ is a stable steady state of (1.1), and a periodic solution emerges as a is increased past 0. For large a these oscillations acquire the character of relaxation oscillations. Thus, $a = 0$ is a bifurcation point. The eigenvalues of the system for a linear perturbation around the origin ($\lambda_{1,2} = \frac{a}{2} \pm i\sqrt{\omega^2 - a^2/4}$) acquire pure imaginary values ($\pm i\omega$) with $\frac{dRe(\lambda_{1,2})}{da} = \frac{1}{2} > 0$ at $a = 0$. A normal form of the equation that preserves these properties can be obtained by doing an appropriate averaging over the fast periodic behavior near the critical point $a = 0$. The resulting nonlinear equation has a simpler structure (that is easier to work with analytically and numerically) and yet maintains the bifurcation characteristics of the original oscillator equation. To carry out such a reduction we rewrite (1.1) as a set of two first-order differential equations, $\dot{x} = \omega y$ and $\dot{y} = -\omega x + (a - x^2)y$. Defining a complex variable $z = x + iy$, these equations may be written as a single equation in terms of z:

$$\dot{z} = -i\omega z + \frac{1}{2}\left[a - \frac{1}{4}(z + \bar{z})^2\right](z - \bar{z}).$$

Let $z = \xi e^{-i\phi}$. (The negative sign introduced in the phase is of no physical significance. The phase flow of the van der Pol is clockwise, but in the biological phase oscillators where equations of the type $\dot{\theta} = \omega$ are common, the phase flow is anti-clockwise and is in the direction of increasing angle.) Then the following two equations emerge for the amplitude and the phase:

$$\dot{\xi} = (a - \xi^2 \cos^2 \phi)\xi \sin^2 \phi,$$
$$\dot{\phi} = \omega + \frac{1}{2}(a - \xi^2 \cos^2 \phi) \sin(2\phi).$$

We now average these two equations over the phase ϕ. The right-hand side of the $\dot{\xi}$ equation is an even function of ϕ, and the average over ϕ from 0 to π results in $(a - \xi^2/4)\xi/2$. The second term on the right-hand side of the $\dot{\phi}$ equation is an odd function of ϕ, and an average over a period of ϕ makes it zero. We call the averaged amplitude and the phase ρ and θ. Hence,

$$\dot{\rho} = \left(a - \frac{1}{4}\rho^2\right)\frac{\rho}{2}, \tag{1.2}$$
$$\dot{\theta} = \omega. \tag{1.3}$$

The behavior of the two eigenvalues of this reduced set of equations at $a = 0$ is the same as that of (1.1) mentioned before. We can also see this by noting from (1.2) and (1.3) that the growth of amplitude for very small perturbations around $\rho = 0$ is proportional to $a/2$ and the frequency of such a growth is ω, identical to the eigenvalue behavior of (1.1). For a positive but near 0, the phase plane orbits of (1.1) are circular just as those for (1.2) and (1.3), but will become distorted for large a. Using ρ and θ, a second-order approximation for the amplitude and phase can be derived that reveals the dependence of the amplitude on the phase and the phase evolution on the amplitude. But we confine our description to the first-order approximation. By redefining $Z(t) = \frac{\rho}{2}e^{i\theta}$, (1.2) and (1.3) can be written as a single equation in the complex variable $Z(t)$, namely,

$$\dot{Z}(t) = (a + i\omega - \mid Z(t) \mid^2)Z(t) \tag{1.4}$$

and which is the final normal form of the equation that we will work with. Equation (1.4) is also widely known as the Stuart–Landau oscillator. Note that this equation shows stable oscillations ($Z(t) = \sqrt{a}e^{i\omega t}$) for $a > 0$ with amplitude $\sqrt{a}$ and a stable rest state ($Z(t) = 0$) for $a < 0$. The value $a = 0$ is the supercritical Hopf bifurcation point. Our minimal model consists of two such oscillators that are linearly (diffusively) coupled to each other and where the coupling is time delayed. The model equations are

$$\dot{Z}_1(t) = (1 + i\omega_1 - \mid Z_1(t) \mid^2)Z_1(t) + K[Z_2(t - \tau) - Z_1(t)], \tag{1.5}$$
$$\dot{Z}_2(t) = (1 + i\omega_2 - \mid Z_2(t) \mid^2)Z_2(t) + K[Z_1(t - \tau) - Z_2(t)], \tag{1.6}$$

where we have chosen $a = 1$ (so that each oscillator in the uncoupled state is in the stable limit cycle state), K is the strength of coupling, and τ is a discrete and constant delay time. As an approximation to a physical system, (1.5) and (1.6) can be viewed as two nonlinear electronic circuits that are resistively coupled to each other. We will study the dynamics of the above system in terms of the frequency difference ($\Delta = \mid \omega_1 - \omega_2 \mid$), the average frequency ($\bar{\omega} = (\omega_1 + \omega_2)/2$), and the coupling strength (K) as a function of the time delay parameter τ. In the absence of time delay, the above set of equations (and its generalizations) have been studied in detail by Aronson et al. [24] to delineate the bifurcation structures and the existence of various collective states. In Fig. 1.1 we have redrawn their bifurcation diagram to illustrate the main features of their analyses. Broadly, the bifurcation diagram may be divided into three regimes: (1) frequencies are identical, $\omega_1 = \omega_2 = \omega$, that is $\Delta = 0$, (2) frequencies are weakly dissimilar (i.e., $0 < \Delta < 2$), and (3) frequencies are very dissimilar (i.e., $\Delta > 2$). For identical intrinsic frequencies ($\Delta = 0$), the coupled oscillators are always synchronized (with no phase delay between the oscillations). This is the only stable solution for any positive and finite coupling strength. The level of K determines how fast the synchronized state is attained from any given set of initial conditions. For weakly dissimilar frequencies ($0 < \Delta < 2$), the oscillators can be found in two different states: phase drift or phase-locked states. A critical value of coupling ($K > \Delta/2$) is required to phase-lock the oscillators. In

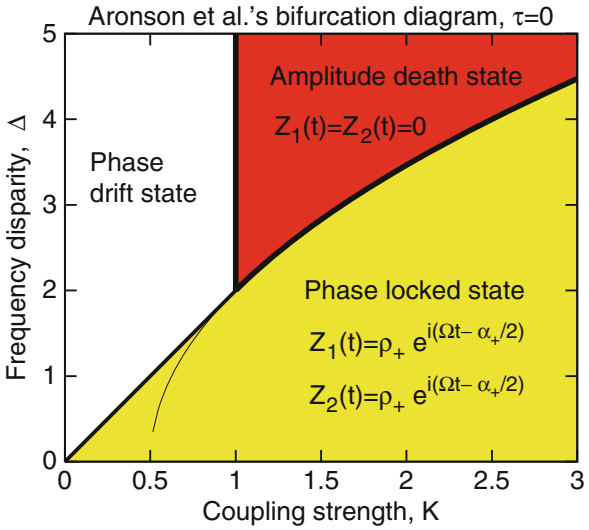

Fig. 1.1 Aronson et al.'s [24] bifurcation diagram of (1.5) and (1.6) for $\tau = 0$. The boundaries of the death state are determined from the eigenvalues of the linearized equations at $Z_{1,2} = 0$: For $\Delta > 2$, $K = 1$ and $\kappa \equiv K = \frac{1}{2}(1 + \Delta^2/4)$ define the boundaries. The stable phase-locked state is the node of symmetric solutions that form a saddle-node pair that emerges on $\Delta = 2K$ and $K < 1$. The saddle merges with the origin on the thin line, κ. The node has the amplitude $\rho_+ = \sqrt{1 - K + \sqrt{K^2 - \Delta^2/4}}$, $\Omega = \bar{\omega}$, and $\alpha_+ = \sin^{-1}(\Delta/2K)$

such phase-locked state, the phase difference between the oscillators is a constant of time and is determined by the coupling strength and the frequency difference. For weak coupling in this regime, a phase drift occurs (i.e., $\theta_1 - \theta_2$ is a function of time and runs from 0 to 2π). In these two regimes, the amplitude of the oscillators does not offer any particularly interesting feature. In the third regime ($\Delta > 2$), however, when the frequency disparity is strong, a third solution, a stable *amplitude death* state, can exist in addition to phase drift and phase-locked states. The level of coupling strength determines the stability of each of these states. For $K < 1$, phase drift occurs. For $K > (1 + \Delta^2/4)/2$, phase-locking occurs. For intermediate K, the amplitude of the oscillators becomes zero. This state is nothing but the stable fixed point state ($Z_{1,2}(t) = 0$) and does not exist for phase-only coupled oscillators (i.e., when the amplitudes of the two oscillators are forced to assume a value of unity while letting the phases to evolve). This state is a reflection of the effect of amplitude on the collective oscillations of the coupled oscillators. The boundaries of various regions can be determined by a stability analysis of these states [24]. We will now study the effect of finite time delay ($\tau \neq 0$) on the characteristics of this phase diagram.

1.2.1 Time delay effects

We rewrite the model Equations (1.5) and (1.6) in polar coordinates by letting $Z_{1,2}(t) = r_{1,2}e^{i\theta_{1,2}}$ to get

$$\dot{r}_1(t) = (1 - K - r_1(t)^2)r_1(t) + Kr_2(t-\tau)\cos[\theta_2(t-\tau) - \theta_1(t)], \tag{1.7}$$

$$\dot{\theta}_1(t) = \omega_1 + K\frac{r_2(t-\tau)}{r_1(t)}\sin[\theta_2(t-\tau) - \theta_1(t)], \tag{1.8}$$

$$\dot{r}_2(t) = (1 - K - r_2(t)^2)r_2(t) + Kr_1(t-\tau)\cos[\theta_1(t-\tau) - \theta_2(t)], \tag{1.9}$$

$$\dot{\theta}_2(t) = \omega_2 + K\frac{r_1(t-\tau)}{r_2(t)}\sin[\theta_1(t-\tau) - \theta_2(t)]. \tag{1.10}$$

This form is more useful for analysis of periodic states whereas the Cartesian form is convenient for linear stability studies, and we will utilize either form as per our needs.

1.2.1.1 Phase-Locked States

Let us consider identical oscillators, that is, $\Delta = 0$, and hence $\omega_1 = \omega_2 \equiv \omega_0$. This is also trivially the average frequency $\bar{\omega}$. Without time delay ($\tau = 0$), the in-phase-locked state is a stable solution. The interactions are instantaneous and do not depend on time history. Hence, any phase mismatch introduced by way of perturbation is transmitted to both the oscillators instantly. Once the perturbation ceases, the oscillators resume their oscillations with their natural frequencies. The coupling coefficient K determines the recovery time window before their natural oscillations

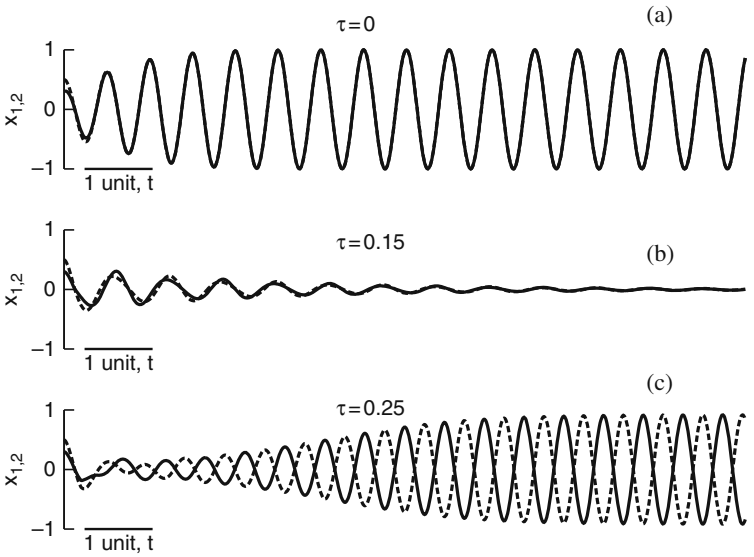

Fig. 1.2 Numerical solutions of coupled identical ($\Delta = 0$) oscillators ((1.5) and (1.6)) at $K = 2$, $\omega_0 = 10$. The initial conditions are $x_1 = 0.3$, $x_2 = 0.5$, $y_1 = 0$, $y_2 = 0$. The delay vectors $Z_{1,2}(t) = 0, \tau < t < 0$. Stable in-phase-locked state is reached quickly for very small or no time delay. Amplitude death is encountered as τ is increased, and the system emerges into an anti-phase-locked state for further increments. Our analysis will reveal multiple regions of amplitude death at larger values of τ

are synchronized. This stable state is also seen in the bifurcation diagram (Fig. 1.1). The evolution of the real components of the two oscillators in this in-phase-locked state are illustrated in Fig. 1.2(a).

For finite τ the interactions are non-instantaneous. Earlier studies on phase coupled oscillators that included time delays predicted multiple frequency states where the oscillators could possess any of several stable frequency states allowed for the given parameter set. The possibility of such multiple states arising due to time delay may be seen directly from (1.7), (1.8), (1.9), (1.10), where the dependence of the derivatives on phases involves sinusoidal functions of τ. We will show that this dependence will lead to transcendental equations for oscillation frequency and thus result in multiple frequency states. For identical oscillators, such multiple frequency states are either in-phase or anti-phase. Multi-stability can occur between in-phase states, anti-phase states, or between in-phase and anti-phase states. For any given state, the frequency of oscillation decreases with increasing τ (Fig. 1.3(b)) as also predicted earlier by other studies [29]. In our example simulating the parameters allow both in-phase and anti-phase states and they exist in different parameter regions for $\tau < 0.3$ (Fig. 1.2(c) and Fig. 1.3(b) and (c)).

The fact that we have amplitude evolutions along with the phase evolutions (see (1.7), (1.8), (1.9), (1.10)) has significance for the existence of these states. The in-phase state at $\tau = 0$ continues to exist for slightly higher levels of τ, but the

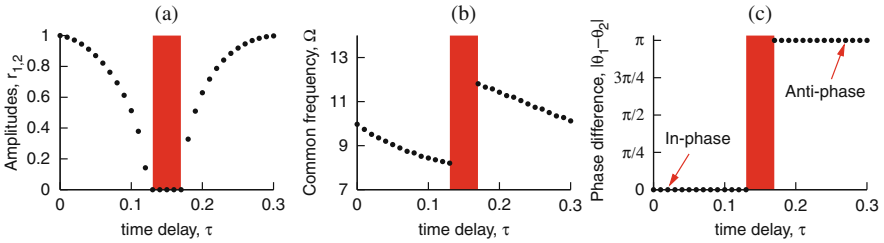

Fig. 1.3 Numerical simulation results of coupled identical ($\Delta = 0$) oscillators ((1.5) and (1.6)) at $K = 2$, $\bar{\omega} = 10$. After initial transients, the amplitudes and frequencies of both the oscillators become constants in time. The solutions are sinusoidal, but the plotted frequencies are the peaks of the Fourier spectrum of the time course of x_1. The phases of the oscillators are computed using $\theta_1 = \tan^{-1}(y_1/x_1)$ and $\theta_2 = \tan^{-1}(y_2/x_2)$. The shaded region is the parameter region of amplitude death along τ

amplitude of the oscillations decreases until it completely becomes zero (Figs. 1.2(b) and 1.3(a)). In this state any damped oscillations might still show an in-phase relationship, but they are transient in nature, and the long-time steady state is the zero amplitude steady state. In fact as τ is increased, these damped oscillations become anti-phase, and above a critical τ, the amplitude of these oscillations becomes non-zero, and a stable anti-phase state emerges (Fig. 1.3). The zero-amplitude state is the region of stability of $Z_{1,2} = 0$ and is the death state. The boundaries of the death state seen in Fig. 1.3 (shaded regions) are the boundaries of the 'death island' which will be discussed later.

We will later on derive the boundaries of the death state by using the eigenvalue analysis. But the emergence of the death and anti-phase solutions and their stability may be derived simply from an empirical observation of the numerical results of Fig. 1.3. Numerical simulations reveal the symmetry of the system. In the in-phase and anti-phase states the amplitudes of both the oscillators are identical and independent of time ($r_1(t) = r_2(t) = r^*$). Their phase evolutions (not shown) are linear growths ($\theta_1(t) = \Omega t + c_1$, $\theta_2(t) = \Omega t + c_2$) of time with a frequency (Ω) that may differ from their intrinsic frequency (ω_0). The quantities c_1 and c_2 are constants in time and depend on the initial conditions. The phase difference of the oscillators is measured by $| c_1 - c_2 |$. In the in-phase state the phase difference is zero and in the anti-phase state it is π. For ease of analysis, we will assume that $c_1 = -\alpha/2$ and $c_2 = \alpha/2$, so that in the in-phase state $\alpha = 0$ and in the anti-phase state $\alpha = \pi$. Let us first substitute in (1.8) and (1.10) the above observations on the amplitudes:

$$\dot{\theta}_1(t) = \omega_0 + K \sin[\theta_2(t-\tau) - \theta_1(t)], \tag{1.11}$$

$$\dot{\theta}_2(t) = \omega_0 + K \sin[\theta_1(t-\tau) - \theta_2(t)]. \tag{1.12}$$

Define $\phi(t) = \theta_2(t) - \theta_1(t)$ and take the difference of the above two equations to get

$$\dot{\phi}(t) = -2K \cos(\Omega\tau) \sin\phi, \tag{1.13}$$

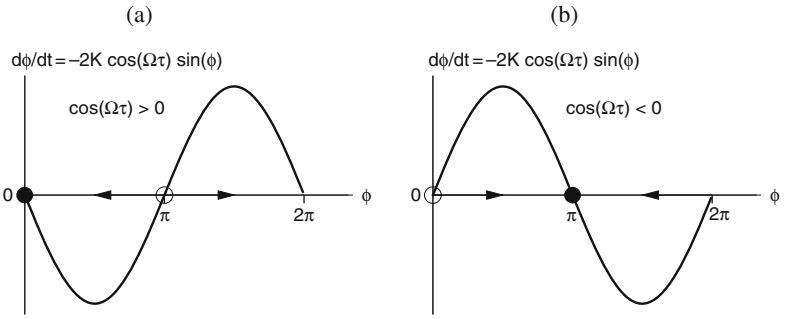

Fig. 1.4 Stability of in-phase and anti-phase solutions is decided by the sign of $\cos(\Omega\tau)$. The filled phase point is the stable solution in each case. For $\cos(\Omega\tau) > 0$ the in-phase solution is stable, and for $\cos(\Omega\tau) < 0$ the anti-phase solution is stable

where we have used the relations $\theta_1(t-\tau) - \theta_1(t) = \theta_2(t-\tau) - \theta_2(t) = -\Omega\tau$ and $\theta_2(t-\tau) - \theta_1(t-\tau) = \theta_2 - \theta_1$. These relations are again derived from the observations that we made above on the phase evolutions in the phase-locked states. We have not yet specified the phase difference α between the oscillators. So this phase difference evolution equation applies for both in-phase and anti-phase states alike. This equation also helps us in understanding the stability of both in-phase and anti-phase states. For $\cos(\Omega\tau) > 0$ (Fig. 1.4(a)), the slope of $\dot{\phi}$ (i.e., the rate of change of the phase difference) is negative, signifying that any brief perturbation from this state will decay to that state in time, as also indicated by the directional flow. Hence, the in-phase state is stable, and the anti-phase state is unstable. But for $\cos(\Omega\tau) < 0$ (Fig. 1.4(b)), the anti-phase state acquires stability and the in-phase state loses its stability.

Does the in-phase state have to become unstable for the anti-phase state to become stable, and vice versa? No. In fact both states can co-exist. This is possible because the frequencies of these two states can be different while still obeying the stability relations shown in Fig. 1.4. The frequencies are in fact determined by solving different transcendental equations involving Ω and τ for the two states. To see this, substitute the in-phase states $\theta_{1,2}(t) = \Omega t$ (i.e., $\alpha = 0$) in (1.11) to obtain a transcendental equation for the in-phase frequencies:

$$f_{\text{in}}(\Omega) = \Omega - \omega_0 + K\sin(\Omega\tau) = 0. \tag{1.14}$$

Similarly, for the anti-phase states, substituting $\theta_{1,2}(t) = \Omega t \mp \pi/2$ in (1.11), another transcendental equation for Ω is obtained for anti-phase frequencies:

$$f_{\text{anti}}(\Omega) = \Omega - \omega_0 - K\sin(\Omega\tau) = 0. \tag{1.15}$$

f_{in} and f_{anti} are plotted as a function of Ω in Fig. 1.5 for sample parameter values. The zeros of these curves are the allowed in-phase or anti-phase frequencies. For small τ only one solution for each state (marked by dots) could be found, but at

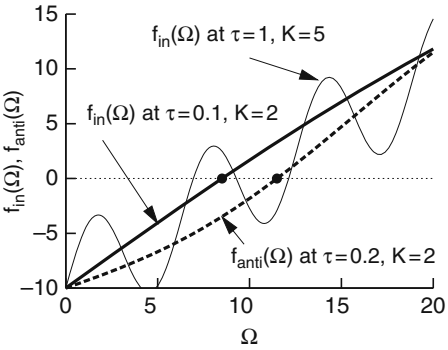

Fig. 1.5 The allowed values of frequencies for in-phase and anti-phase states are determined by solving for the zeros of the functions $f_{\rm in}(\Omega)$ and $f_{\rm anti}(\Omega)$. These two curves plotted as a function of Ω at $\tau = 0.1$, $K = 2$, show single solutions for in-phase and anti-phase states (marked by filled bullets). At large K, the curves show bigger amplitude oscillations and at longer τ they show more wiggles in any given Ω-window. Both these features help establish multiple frequency states for both in- and anti-phase states as seen, for example, by the multiple zeros of $f_{\rm in}$ at $\tau = 1$ and $K = 5$:

larger τ and/or K, multiple zeros could result, correspondingly yielding multiple frequencies.

The stability of any one state with frequency Ω, as stated above, depends on the sign of $\cos(\Omega\tau)$. This stability analysis is illustrated pictorially for an in-phase and an anti-phase branch in Fig. 1.6. The frequencies of the in-phase and anti-phase states are obtained by solving $f_{\rm in} = 0$ and $f_{\rm anti} = 0$ and are plotted as a function of τ. The stable in-phase branch corresponding to $\cos(\Omega\tau) > 0$ (Fig. 1.6(a)) and the stable anti-phase branch corresponding to $\cos(\Omega\tau) < 0$ (Fig. 1.6(b)) are marked with filled dots. The unfilled dots indicate unstable portions of the frequency branches. We might already have here a bistable region between in-phase and anti-phase states. However, the amplitudes of each of these states must also be considered and verified whether these states assume physically acceptable (i.e., real and positive) values.

The amplitude of the in-phase state is obtained by substituting $r_1(t) = r_2(t) = r_{\rm in}$ and $\theta_{1,2}(t) = \Omega t$ in (1.7):

$$r_{\rm in}^2 = 1 - K + K\cos(\Omega\tau). \tag{1.16}$$

The right-hand side of this equation is real and positive only when $\cos(\Omega\tau) > 1 - 1/K$. Since $\cos(\Omega\tau)$ is a smooth function of its argument, in fact, as τ is increased the amplitude gradually decreases to 0 on the curve

$$\cos(\Omega\tau) = 1 - \frac{1}{K} \tag{1.17}$$

and $r_{\rm in}^2$ remains unphysically negative for $0 < \cos(\Omega\tau) < 1/K - 1$ (shown by the guiding lines in Fig. 1.6(a)). This boundary where the amplitude becomes 0, however, marks the transition of the in-phase state with finite amplitude to a

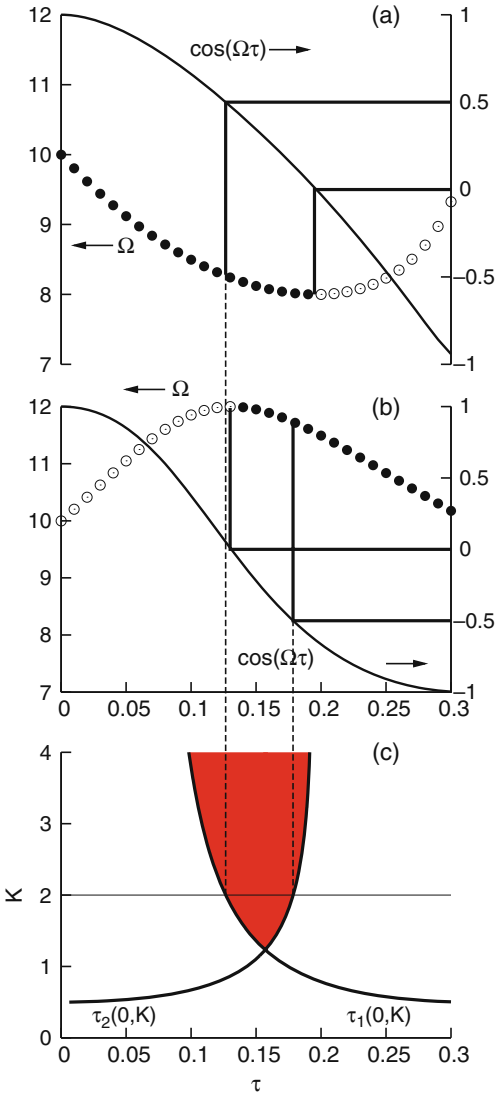

Fig. 1.6 Frequency branches of in-phase-locked (**a**) and anti-phase (**b**)-locked states obtained by solving $f_{\text{in}} = 0$ and $f_{\text{anti}} = 0$ at $K = 2$ and $\omega_0 = 10$. The *filled circles* indicate the stable states in each case corresponding to the stability conditions shown in Fig. 1.4. The *guiding lines* enclose parameter regions where the amplitudes of the in-phase and anti-phase states have unphysical values. The left boundary of this region in the in-phase state and the right boundary in the anti-phase state correspond to the parameter values where the amplitudes become 0. These boundaries match exactly with those (**c**) ($\tau_1(0, K)$ and $\tau_2(0, K)$) obtained from eigenvalue analysis. Here the match must be at $K = 2$. The shaded region is the death island region and extends beyond the ordinate boundary

zero-amplitude state or the death state. We will in fact see from eigenvalue analysis that this is one of the death region (death island) boundaries. We plot the death boundary $\tau_1(0, K)$ corresponding to $\omega_0 = 10$ (to be derived later) and find an exact match between a death island boundary and that predicted by the above equation (Fig. 1.6(c)). Similarly, we examine the amplitude of the anti-phase state by substituting $r_1(t) = r_2(t) = r_{\text{anti}}$ and $\theta_{1,2}(t) = \Omega t \mp \pi/2$ in one of the phase evolution equations, say (1.8), and obtain

$$r_{\text{anti}}^2 = 1 - K - K\cos(\Omega\tau). \tag{1.18}$$

The right-hand side of this equation is real and positive only when $\cos(\Omega\tau) < 1 - 1/K$. Again, this function varies smoothly with its argument and becomes zero on the curve

$$\cos(\Omega\tau) = \frac{1}{K} - 1 \tag{1.19}$$

and remains unphysically negative for $1/K - 1 < \cos(\Omega\tau) < 0$ (shown by the guiding lines in Fig. 1.6(b)). This boundary where the amplitude of the anti-phase oscillations becomes 0 matches exactly with the boundary $\tau_2(0, K)$ derived from the eigenvalue analysis (Fig. 1.6(c)).

1.2.1.2 Amplitude Death

We will now study the amplitude death region and show how to derive these boundaries systematically from the characteristic equation. The amplitude death region is the region of stability of the trivial solution: $Z_{1,2} = 0$, and the eigenvalues of this state determine the boundaries of the amplitude death both for identical and for non-identical oscillators. The characteristic equation we obtain will be transcendental in nature and can possess an infinite number of eigenvalues. The amplitude death region is determined from the parameters in the characteristic equation by insisting that all the eigenvalues have negative real parts. For example, if $\lambda = \alpha + i\beta$ (where α and β are real) represents all the eigenvalues of the system, the stable death region is determined by the condition $\alpha < 0$ and the boundary of the death region is determined by $\alpha = 0$. Owing to the fact that we will have a transcendental characteristic equation (and hence multiple solutions; see, for example, Fig. 1.5), this death boundary condition results in multiple curves in the parameter space, leading to the possibility of multiple regions of death state.

The characteristic equation of (1.5) and (1.6) is obtained by linearizing these equations around $Z_{1,2} = 0$ and substituting $Z_{1,2}(t) = Z_{1,2}(0)e^{\lambda t}$. The resultant matrix on the right-hand side of the equations is

$$A = \begin{bmatrix} 1 - K + i\omega_1 & Ke^{-\lambda\tau} \\ Ke^{-\lambda\tau} & 1 - K + i\omega_2 \end{bmatrix}. \tag{1.20}$$

The characteristic equation is nothing but $\det(A - \lambda I) = 0$, where I is the 2×2 unit matrix. By expanding this equation, we can write it as the following transcendental equation:

$$(a - \lambda + i\omega_1)(a - \lambda + i\omega_2) - K^2 e^{-2\lambda\tau} = 0, \tag{1.21}$$

where $a = 1 - K$. Complete analytical solutions of such transcendental equations are not generally available, but we can use the equations to obtain critical curves bounding the stable (death) region. We first show the stable regions between non-identical oscillators and then derive boundaries for identical oscillators. As outlined above, we obtain critical curves by seeking that the real parts of the eigenvalues are zero. On these curves, a pair of eigenvalues cross into right half of the eigenvalue plane (i.e., a stability switch could take place). Since we already know the region of stability in the absence of time delay, we increase τ slightly and look for the critical curves that are nearest to this region. Across these curves, stability of the rest state is lost, and thus they provide the boundaries of the death region. On the critical curves, let $\lambda = i\beta$. Substituting this in the above equation and separating the real and imaginary components, we obtain $(\beta - \bar{\omega})^2 - \Delta^2/4 - a^2 + K^2 \cos(2\beta\tau) = 0$ and $2a(\beta - \bar{\omega}) - K^2 \sin(2\beta\tau) = 0$. These two equations may be used to compute critical curves in (K, Δ) plane by eliminating β. For convenience we write them as follows:

$$F = (\beta - \bar{\omega})/\sin(2\beta\tau), \tag{1.22}$$

$$K \equiv K_{\pm} = -F \pm \sqrt{F^2 + 2F}, \tag{1.23}$$

$$\Delta^2 = -4a^2 + 4(\beta - \bar{\omega})^2 + 4K^2 \cos(2\beta\tau). \tag{1.24}$$

By choosing β from intervals $I_n = (n\pi/2\tau, (n+1)\pi/2\tau)$, portions of curves are obtained in (K, Δ) plane. We term these curves as $S_{\pm}$ depending on the sign being used to compute K in (1.23). For $\bar{\omega} = 10$ we show in Fig. 1.7 these critical curves in the (K, Δ) plane using the interval I_0. S_+ curves are drawn in dashes and S_- in continuous lines. The shaded region is the amplitude death region. For τ very small, the region is closer to that of Aronson et al.'s (Fig. 1.1). But as τ is increased, the region expands toward smaller values of Δ, and for a range of τ values, it displays amplitude death state along $\Delta = 0$ axis. That is, identical oscillators can exhibit amplitude death state if appropriate time delay is introduced in their interactions.

We will now be interested in this phenomenon of amplitude death for $\Delta = 0$ and wish to quantify the region of death for various τ by finding the critical curves that define the boundaries of the death region in (K, τ) plane. To do this, it is best to consider (1.21) and substitute $\omega_1 = \omega_2 = \omega_0$ there. This gives a set of two simpler characteristic equations

$$\lambda = 1 - K + i\omega_0 \pm K e^{-\lambda\tau}, \tag{1.25}$$

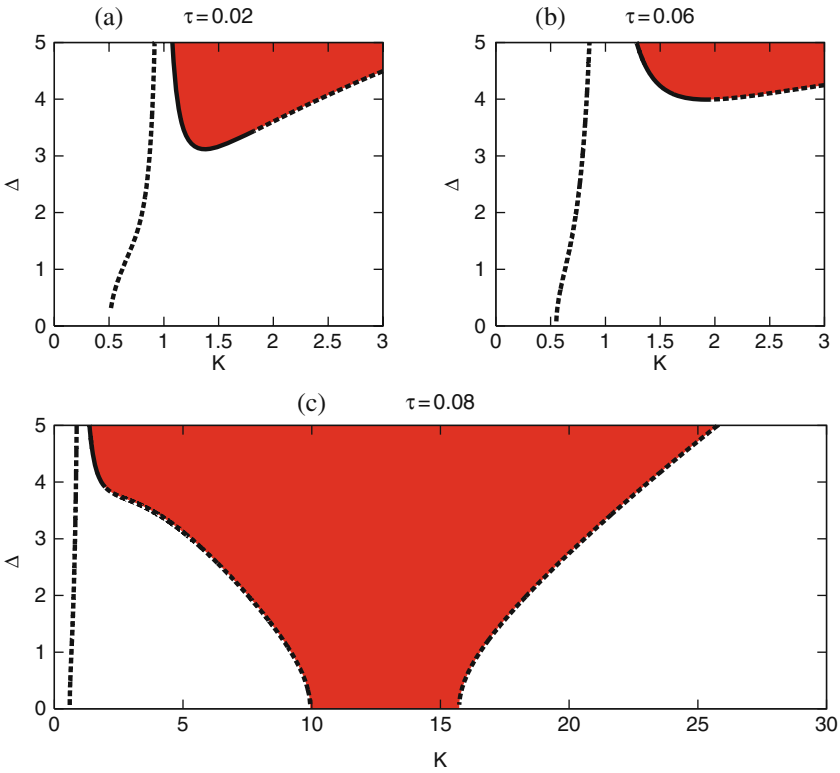

Fig. 1.7 Amplitude death region (*shaded*) shown for three values of τ at $\bar{\omega} = 10$. The boundaries are the curves S_- (*solid lines*) and S_+ (*dashed lines*) drawn by eliminating β from (1.22), (1.23) and (1.24)

which can now be analyzed for critical curves. Again for criticality, substitute $\lambda = i\beta$. We obtain, by separating the real and imaginary parts, the following two equations which can be used to eliminate β and obtain curves, or death island boundaries, in (τ, K) plane. Using $+$ sign,

$$\cos(\beta\tau) = 1 - \frac{1}{K}, \tag{1.26}$$

$$\beta - \omega_0 + K\sin(\beta\tau) = 0. \tag{1.27}$$

These are exactly the same equations we obtained earlier for in-phase-locked states (1.14), and the condition for amplitude of that state to be zero (1.17), confirming that the in-phase state indeed emerges from the death state on this critical curve. Using $-$ sign, we obtain

$$\cos(\beta\tau) = \frac{1}{K} - 1, \tag{1.28}$$

$$\beta - \omega_0 - K\sin(\beta\tau) = 0. \tag{1.29}$$

These are exactly the same equations we obtained earlier for anti-phase-locked states (1.15), and the condition for amplitude of that state to be zero (1.19), confirming that an anti-phase state emerges from the death state on this critical curve. The value of β can be expressed independently of the sinusoidal function in both the above cases. Inverting the cosine functions results in multiple values for τ as a function of K. Each of these curves is a critical curve across which pairs of eigenvalues cross into the right half eigenvalue plane. A numerical ordering of these curves reveals [32, 33] that the death island boundaries are given by

$$\tau_1 \equiv \tau_1(n,K) = \frac{n\pi + \cos^{-1}(1-1/K)}{\omega_0 - \sqrt{2K-1}}, \tag{1.30}$$

$$\tau_2 \equiv \tau_2(n,K) = \frac{(n+1)\pi - \cos^{-1}(1-1/K)}{\omega_0 + \sqrt{2K-1}}. \tag{1.31}$$

We plot these curves in Fig. 1.8 for $\omega_0 = 30$ and shade the regions of amplitude death. The death regions are multiple in number at this value of ω_0. A more detailed analysis [32, 33] also reveals that the eigenvalues indeed cross these boundaries from inside to outside as we expect.

1.3 *N*-Oscillator Models

With the insights gained from the analysis of the minimal model of just two coupled oscillators, we will now try to study the collective states of a more complex system where we have a large number N of coupled oscillators. When the number of oscillators is large ($N > 2$), the mutual coupling can occur in a variety of ways.

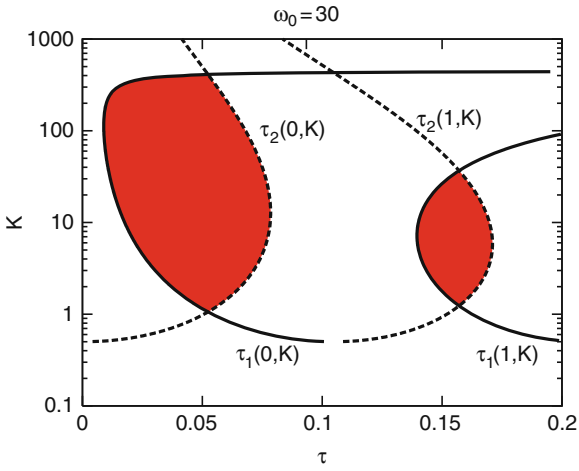

Fig. 1.8 Two of the three death islands are shown for $\omega_0 = 30$

One simple way is to connect each oscillator to every other oscillator with a constant coupling strength. Such a system is called a globally coupled system or more commonly as a mean field model. Another widely used coupling scheme is that of nearest neighbor coupling which is often referred to as diffusive coupling. A more generalized form of coupling that reduces to the above two in limiting cases is that of non-local coupling in which the coupling extends over a wider spatial extent but with a varying strength. In this section we will introduce time delay coupled versions of all these three models and discuss the effect of time delay on their collective states. We will restrict ourselves to one-dimensional configurations (for the locally and non-locally coupled systems) which are simpler to analyze. Our present discussion will be primarily based on the work carried out in [33, 35–37].

1.3.1 Global Coupling

Making a straightforward generalization of (1.5) and (1.6), one can describe a system of N globally coupled Stuart–Landau oscillators (with a linear time-delayed coupling) by the following set of model equations:

$$\dot{Z}_j(t) = (1 + i\omega_j - \mid Z_j(t) \mid^2)Z_j(t) + \frac{K'}{N}\sum_{k=1}^{N}[Z_k(t-\tau) - Z_j(t)] - \frac{K'}{N}[Z_j(t-\tau) - Z_j(t)], \tag{1.32}$$

where $j = 1, \ldots, N$, $K' = 2K$, is the coupling strength and τ is the delay time. The coupling term on the right-hand side now has a summation up to N, ensuring coupling of an individual oscillator to every other one in the system, whereas the last term has been introduced to subtract the self-coupling term from the summation. In the absence of time delay, such a mean field model has been studied extensively in the past in [5, 20, 25, 27] in order to delineate the various stationary and non-stationary states of the system including phase-locked states, amplitude death, phase drift states, Hopf oscillations, and even chaotic states. We will examine the effect of time delay on some of these states. For this it is convenient to define an order parameter, defined as,

$$\bar{Z} = Re^{i\phi} = \frac{1}{N}\sum_{j=1}^{N} Z_j(t), \tag{1.33}$$

where R and ϕ denote the amplitude and phase of the centroid. In a large N model the order parameter provides a time-asymptotic measure of the coherence (collective aspects) of the system in both a qualitative and a quantitative fashion. When $R = 0$ (in the large time limit) the system can be considered to be in an incoherent state whereas $R = 1$ marks a totally synchronized or 'phase-locked' state. Any value

in between indicates that the system is in a partially synchronized state. The order parameter is also capable of displaying signatures of non-stationary states like chaos and large amplitude Hopf oscillations through its temporal behavior [25, 27]. Using the order parameter, the model equations can be rewritten more compactly as

$$\dot{Z}_j(t) = (1 - K'd + i\omega_j - \mid Z_j(t) \mid^2)Z_j(t) + K'\bar{Z}(t-\tau) - \frac{K'}{N}Z_j(t-\tau), \quad (1.34)$$

where $d = 1 - 1/N$. We will now study the stability of the origin of these equations (for examining the amplitude death state) and also discuss the phase-locked states of the system.

1.3.1.1 Amplitude Death

The stability of the origin can be determined as before by doing a linear perturbation analysis around $Z_j = 0$ in (1.32). Assuming the perturbations to vary in time as $e^{\lambda t}$, the characteristic matrix of (1.32) is given by

$$B = \begin{bmatrix} l_1 & f & \cdots & f \\ f & l_2 & \cdots & f \\ \vdots & \vdots & \ddots & \vdots \\ f & f & \cdots & l_N \end{bmatrix}, \quad (1.35)$$

where $l_n = 1 - K'd + i\omega_n$ and $f = \frac{K'}{N}\, e^{-\lambda\tau}$. The eigenvalue problem can also be cast in terms of another matrix $C = B + (K'd - 1)I$ (with I being the identity matrix), such that if μ is the eigenvalue of C then it is related to λ by the relation $\mu = \lambda + (K'd - 1)$. The eigenvalue equation $\det(C - \mu I) = 0$ can be compactly expressed as a product of two factors:

$$\left[\prod_{k=1}^{N}(i\omega_k - \mu - f)\right]\left[1 + f\sum_{j=1}^{N}\frac{1}{i\omega_j - \mu - f}\right] = 0. \quad (1.36)$$

As discussed by Matthews and Strogatz [38, 27], for the no-delay case, solutions of the first factor represent the continuous spectrum of the system whereas the second factor provides the discrete spectrum. The characteristic Equation (1.36) is difficult to solve analytically or even numerically when N is large. We will confine ourselves to the case of N identical oscillators where a simple analysis is possible and which will also allow us to seek a generalization of the $N = 2$ result discussed in the previous section. For N identical oscillators the frequency distribution of the system can be expressed as a delta function

$$g(\omega) = \delta(\omega - \omega_0), \quad (1.37)$$

where ω_0 is the natural frequency of each oscillator. With such a distribution the eigenvalue equation can be simplified to the form

$$\lambda = \left\{1 - K'd + i\omega_0 + K'de^{-\lambda\tau},\ \ 1 - K'd + i\omega_0 - \frac{K'}{N}e^{-\lambda\tau}\right\}, \tag{1.38}$$

in which the second eigenvalue has a degeneracy of $N - 1$. Using both the eigenvalue equations and the procedure described for the $N = 2$ case, one can obtain the following set of critical curves:

$$\tau_a(n, K) = \frac{2n\pi + \cos^{-1}\left[1 - \frac{1}{K'd}\right]}{\omega_0 - \sqrt{2K'd - 1}}, \tag{1.39}$$

$$\tau_b(n, K) = \frac{2(n+1)\pi - \cos^{-1}\left[1 - \frac{1}{K'd}\right]}{\omega_0 + \sqrt{2K'd - 1}}, \tag{1.40}$$

$$\tau_c(n, K) = \frac{2(n+1)\pi - \cos^{-1}\left[\frac{1-K'd}{K'(1-d)}\right]}{\omega_0 - \sqrt{[K'(1-d)]^2 - (K'd-1)^2}}, \tag{1.41}$$

$$\tau_d(n, K) = \frac{2n\pi + \cos^{-1}\left[\frac{1-K'd}{K'(1-d)}\right]}{\omega_0 + \sqrt{[K'(1-d)]^2 - (K'd-1)^2}}. \tag{1.42}$$

In contrast to the $N = 2$ case, the family of curves is now four instead of two, and they are functions of the parameter N. It is easy to check that for $N = 2$, the curves $\tau_a(n, K)$ and $\tau_c(n, K)$ combine to give $\tau_1(n, K)$ and $\tau_b(n, K)$ and $\tau_d(n, K)$ combine to give $\tau_2(n, K)$ which were obtained in the earlier section. We show some typical death island regions in Fig. 1.9(a) for various values of N as obtained from the critical curves (1.39), (1.40), (1.41) and (1.42) with $n = 0$. The sizes of the islands are seen to vary as a function of N and to approach a saturated size as $N \to \infty$. The existence of these regions has also been independently confirmed by direct numerical solution of the coupled oscillator equations [33]. Thus, the phenomenon of time delay-induced death for identical oscillators happens even for an arbitrarily large number of oscillators and is a generic property of our coupled oscillator system. As in the $N = 2$ case these death islands can also show multiple connectedness for higher values of ω_0 which is a characteristic feature of delay equations.

1.3.2 Nearest Neighbor Coupling

We now look at a local coupling model in which each oscillator is coupled only to its next nearest neighbor. The summation term on the right-hand side of (1.32) then collapses to just two terms and the model equations have the form

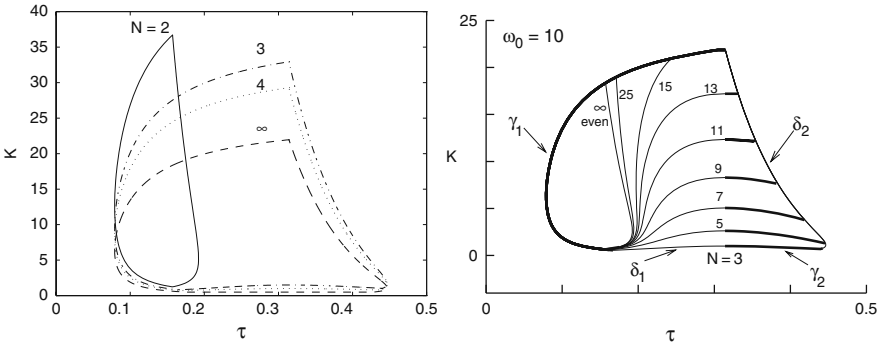

Fig. 1.9 Death islands for global and nearest neighbor couplings. ($\omega_0 = 10$) (a) Death island regions for oscillators with global coupling [32, 33]. (b) Death island regions for oscillators with nearest neighbor coupling. All even number of oscillators have a single death island region that is independent of the number of oscillators. The odd number of oscillators are bounded by four curves when $N \leq 13$ and two curves otherwise. These two curves merge in the infinite limit with the curves that represent the even number of oscillators [35]. For $N \leq 13$, $\gamma_1 = \tau_b(0, K)$ at $R_j = 1$, $\gamma_2 = \tau_b(0, K)$ at $R_{j=(N+1)/2}$, $\delta_1 = \tau_a(0, K)$ at $R_{j=(N+1)/2}$, $\delta_2 = \tau_a(1, K)$ at $R_{j=1}$, and for $N \geq 15$, $\gamma_1 = \tau_b(0, K)$ at $R_{j=1}$, and $\delta_1 = \tau_a(0, K)$ at $R_{j=(N+1)/2}$

$$\frac{\partial Z_j}{\partial t} = (1 + i\omega_j - | Z_j |^2)Z_j + K[Z_{j+1}(t-\tau) - Z_j(t)] + K[Z_{j-1}(t-\tau) - Z_j(t)], \tag{1.43}$$

where the notation is as before. We will simplify this model further by considering only identical oscillators (setting all $\omega_j = \omega_0$) and assuming the oscillators to be arranged in a closed ring. We choose identical oscillators in order to continue our exploration of the death state for the case where there is no frequency dispersion and the ring configuration allows application of periodic boundary conditions when considering phase-locked states. The model equation then has the form

$$\frac{\partial Z_j}{\partial t} = (1 + i\omega_0 - | Z_j |^2)Z_j + K[Z_{j+1}(t-\tau) - Z_j(t)] + K[Z_{j-1}(t-\tau) - Z_j(t)]. \tag{1.44}$$

Note that unlike the global coupling case there is now a spatial dependence in the coupling and therefore the geometrical arrangement of the oscillators matters. This additional dimension introduces new equilibrium states in the system such as traveling waves and in higher dimensions spiral patterns or scroll waves. For $\tau = 0$ one can also make an interesting connection to a well-known nonlinear dynamical equation, namely the complex Ginzburg–Landau equation (CGLE). To see this one can take the limit where the spacing between two oscillators, a, goes to zero, so that $Z_j = Z(ja) \to Z(x)$ where x is a continuum variable. Then (1.44) reduces to

$$\frac{\partial Z(x,t)}{\partial t} = (1 + i\omega_0 - |Z(x,t)|^2)Z(x,t) + K\frac{\partial^2 Z(x,t)}{\partial x^2}, \tag{1.45}$$

where K has been rescaled as K/a^2. This equation has been widely studied and has a rich variety of nonlinear solutions that have found a number of interesting applications.[1] We will return to a more generalized form of this equation later in the chapter. We continue now with the exploration of the amplitude death and phase-locked solutions of (1.44).

1.3.2.1 Amplitude Death

To obtain the conditions for the existence of the death region and to determine its location in parameter space, we resort as usual to a linear perturbation analysis about the origin. Applying periodic boundary conditions (because of the assumed closed chain configuration) we can get the following eigenvalue equation:

$$\prod_{j=1}^{N}\left(\lambda + 2K - 1 - i\omega_0 - Ke^{-\lambda\tau}U_j - Ke^{-\lambda\tau}U_j^{N-1}\right) = 0,$$

where $U_j = \mathrm{e}^{i2\pi(j-1)/N}$ are the Nth roots of unity. Since $U_j + U_j^{N-1} = U_j + U_j^{-1} = 2\cos[(j-1)2\pi/N]$, the above equation can be further simplified to

$$\prod_{j=1}^{N}\left(\lambda + 2K - 1 - i\omega_0 - 2K\cos[(j-1)2\pi/N]\mathrm{e}^{-\lambda\tau}\right) = 0. \tag{1.46}$$

The above equation has to be complemented by its conjugate equation in order to obtain a complete set of eigenvalue equations. We notice that for $\tau = 0$, (1.46) always admits at least one unstable eigenvalue, namely $\lambda = 1 + i\omega_0$. This means that identical oscillators that are locally coupled cannot have an amplitude death state in the absence of time delay, an echo of our earlier results for $N = 2$ and N globally coupled oscillators. In the presence of finite delay, we adopt the same standard procedure that we used earlier for the global coupling case, namely that of determining the marginal stability condition to identify the critical curves. Before we do that, it is worthwhile pointing out another essential and interesting difference from the global coupling case, namely, if N is a multiple of 4 then some of the factors of (1.46) have no explicit τ dependence since for them $R_j = 2\cos[(j-1)2\pi/N] = 0$. Consider the case of $N = 4$ and $j = 2,\ 4$, for which the eigenvalue equation becomes $\lambda = 1 - 2K \pm i\omega_0$, and the only criticality condition is then given by $K = 1/2$. Thus, the stable region lies on the side of the parameter space that obeys $K > 1/2$. For other values of R_j, the death island boundaries can be determined by a marginal

[1] In its most general form, the CGL equation is of the form $\frac{\partial Z(x,t)}{\partial t} = (1 + i\omega_0 - (1 + ib)|Z(x,t)|^2)Z(x,t) + K(1 + ia)\frac{\partial^2 Z(x,t)}{\partial x^2}$, where a and b are real quantities.

stability analysis, and the expressions for the critical curves in the (τ, K) plane are given by

$$\tau_a(n,K) = \begin{cases} \dfrac{2n\pi - \cos^{-1}\left[(2K-1)/KR_j\right]}{\omega_0 + \sqrt{K^2R_j^2 - (2K-1)^2}}, & R_j > 0, \\ \dfrac{(2n+1)\pi - \cos^{-1}\left[(2K-1)/K\left|R_j\right|\right]}{\omega_0 + \sqrt{K^2R_j^2 - (2K-1)^2}}, & R_j < 0, \end{cases} \tag{1.47}$$

$$\tau_b(m,K) = \begin{cases} \dfrac{2m\pi + \cos^{-1}\left[(2K-1)/KR_j\right]}{\omega_0 - \sqrt{K^2R_j^2 - (2K-1)^2}}, & R_j > 0, \\ \dfrac{(2m+1)\pi + \cos^{-1}\left[(2K-1)/K\left|R_j\right|\right]}{\omega_0 - \sqrt{K^2R_j^2 - (2K-1)^2}}, & R_j < 0, \end{cases} \tag{1.48}$$

where n and m are integers. For a detailed analysis of these curves, which includes determination of useful bounds on K for ordering and finding the degeneracies of the critical curves, we refer the reader to [35]. The essential features of the death islands in this system can be gathered from Fig. 1.9(b), where they have been plotted for different values of N. One striking difference is that the size and shape of the death island is now determined by the odd or even property of the number of oscillators N. For an even number of oscillators there is a single death region, whereas for an odd number of oscillators the boundary of the death region depends on the value of N. We illustrate the death states for a sample number of even ($N = 4$) and odd ($N = 5$) nearest neighbor coupled oscillators in Fig. 1.10. The death state for $N = 4$ is surrounded by an in-phase state on the left and an anti-phase state that has neighboring oscillators π out of phase on the right. The death state for $N = 5$ on the other hand has an in-phase state on either side. These differences in the death island widths for even- and odd-numbered oscillators can be traced primarily to the behavior of the eigenvalues of the lowest permitted perturbation wave numbers. As N becomes large, the smallest perturbation mode for the N odd case gets closer to π and the death island boundaries of the two cases become indistinguishable. The size of the death island, for the odd case, decreases as N increases and finally asymptotes to the single ($N =$ even) island as $N \to \infty$. This asymmetry is intimately related to the nature of the coupling and as we will see later it disappears when we change the coupling to a non-local one.

1.3.2.2 Phase-Locked States

As mentioned briefly before, the spatial dependence of the coupling provides for a larger class of equilibrium states in a dispersively coupled system as compared to the globally coupled system. In particular plane wave states, which are characterized

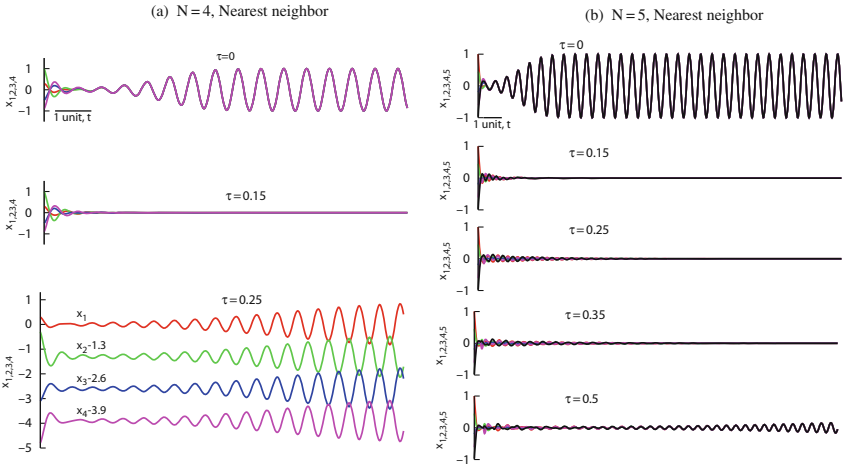

Fig. 1.10 (**a**) A nearest neighbor coupled network of four identical oscillators showing in-phase, death, and then anti-phase patterns as τ is increased, $K = 2$ and $\omega_0 = 10$. The initial conditions are $x_1 = 0.3$, $y_1 = 0$, $x_2 = 1$, $y_2 = 0$, $x_3 = -0.5$, $y_3 = 0$, $x_4 = -0.9$, and $y_4 = 0$. The time history vectors $Z_{1,2,3,4} = 0$. (**b**) A globally coupled network of five identical oscillators showing in-phase, death, and in-phase transitions as τ is increased. Time courses of the real parts of $Z_{1,2,3,4,5}$ are plotted for different τ at $K = 5$ (different than that in (**a**)) and $\omega_0 = 10$. Initial conditions are $x_1 = 1$, $y_1 = 0$, $x_2 = 0.45$, $y_2 = 0$, $x_3 = -0.2$, $y_3 = 0$, $x_4 = -0.61$, $y_4 = 0$, $x_5 = -0.97$, and $y_5 = 0$. The time history vectors $Z_{1,2,3,4,5} = 0$

by a frequency as well as a wave number, are one such possibility. Equation (1.44) admits plane wave solutions of the form

$$Z_j = Re^{i(jka+\omega t)}, \tag{1.49}$$

where a is the distance between any two adjacent oscillators and k is the wave number such that $-\pi \leq ka \leq \pi$. The values of ka are discrete due to the constraint imposed by the periodic boundary conditions, namely that $Z_{N+1} = Z_1$ and $Z_0 = Z_N$. This condition requires that we satisfy $e^{iNka} = 1$ which gives $Nka = 2m\pi$, $m = 0, 1, \ldots, N-1$, that is,

$$ka = m\frac{2\pi}{N}, \quad m = 0, 1, \ldots, N-1. \tag{1.50}$$

Thus, the various phase-locked states are now labeled by their characteristic wave number values. The wave numbers are further related to the frequencies of the states through a dispersion relation which can be obtained by substituting (1.49) in (1.44):

$$i\omega = 1 + i\omega_0 - R^2 + 2K\left[\cos(ka)e^{-i\omega\tau} - 1\right]. \tag{1.51}$$

Separating the real and imaginary parts of the above relation we get

$$\omega = \omega_0 - 2K\sin(\omega\tau)\cos(ka), \tag{1.52}$$

$$R^2 = 1 - 2K + 2K\cos(\omega\tau)\cos(ka). \tag{1.53}$$

It is interesting at this point to compare the above dispersion relation to the plane wave dispersion relation of the CGLE. We can obtain such a dispersion relation by substituting $Z(x,t) = R_{CGL} \exp(ikx - i\omega_{CGL}t)$ in (1.45) to get

$$\omega_{CGL} = \omega_0, \tag{1.54}$$

$$R_{CGL}^2 = 1 - K(ka)^2, \tag{1.55}$$

where we have replaced K by its scaled value. Equations (1.54) and (1.55) can also be obtained from (1.52) and (1.53) by putting $\tau = 0$ and expanding the $\cos(ka)$ term in (1.53) by taking the long wavelength limit of $ka \ll 1$. The two sets of dispersion relations show interesting differences. First of all their domains of validity are different: (1.52) and (1.53) are valid for any arbitrary value of N whereas (1.54) and (1.55) are strictly valid only in the continuum limit (i.e., $N \to \infty$). The ka spectrum is therefore a continuous one for the CGLE whereas in our model they are discrete and also depend on the value of N. For $\tau = 0$, (1.52) and (1.54) become identical, but (1.53) reduces to

$$R^2 = 1 - 2K + 2K\cos(ka) = 1 - 4K\sin^2(ka/2). \tag{1.56}$$

Since $R^2 > 0$ is a necessary condition for a plane wave state to exist, we see that for a given value of K the domain of existence is considerably reduced in the case of the CGLE as compared to the discrete model equations. As an example, at $K = 1/4$, the discrete model allows all modes from 0 to π to exist, whereas the continuum model has an upper cutoff at $ka = 2.0$. For $K > 1/4$ one has cutoff regions in the discrete model as well that are defined by the expression

$$f_1 = \cos^{-1}(1 - 1/2K) < ka < f_2 = 2\pi - \cos^{-1}(1 - 1/2K). \tag{1.57}$$

From (1.57) it is clear that for $K > 1/4$ the anti-phase-locked state ($ka = \pi$) is now no longer a permitted state. In the presence of time delay the existence region is defined by a more complex relation since it is now not only a function of ka (for a given value of K) but also depends on ω which is a solution of the transcendental equation (1.52). Thus, time delay can bring about interesting modifications such as enabling certain forbidden states (of the non-delayed system) to exist and in general reshaping the existence domain significantly. In addition, as we saw in the two oscillator model, the transcendental character of the dispersion relation can introduce additional branches of collective oscillations. A detailed analysis of some of these features are available in [35]. In Fig. 1.11(a) we have illustrated some of the salient findings of [35] by showing the existence regions of plane wave states for some special cases. To delineate the general existence regions which are now complicated functions of ka, K, and τ, one needs to have a simultaneous solution of (1.52) and (1.53). To appreciate the constraints imposed by (1.52) in Fig. 1.11(b) we have plotted the solution (ω vs. ka) for various values of τ and for a fixed value of ω_0 and K. For $\tau = 0$, the values of ka are constrained to be in the range $(|ka|) < \cos^{-1}(1 - 1/2K)$. At $K = 1$, the phase-locked patterns that have wave

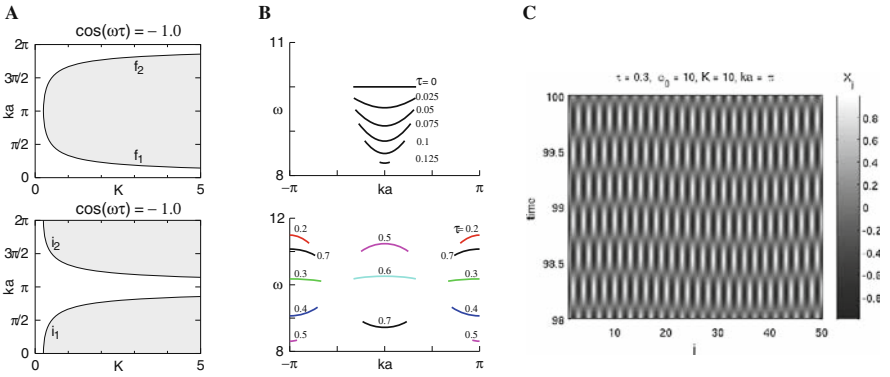

Fig. 1.11 (**a**) Allowed (*unshaded*) and forbidden (*shaded*) wave modes in the presence of time delay for two values of $\cos(\omega\tau)$. (**b**) Dispersion relation between allowed wave numbers and the corresponding frequency shown as τ is gradually increased, $K = 1$ and $\omega_0 = 10$. A range of τ values is forbidden. (**c**) A numerical example of out-of-phase state shown for $N = 50$ oscillators by plotting the level of the real component of Z_j as a function of the oscillator number j [35]

numbers less than $\pi/3$ are allowed, and all of them have an identical frequency. As τ is increased the frequency of oscillation decreases for small τ, and the dispersion relation acquires a nonlinear parabolic character. As τ is further increased, depending on the actual value of K, there are bands in τ values where no modes exist. The shrinking and disappearance of the dispersion curve at $ka = 0$ beyond $\tau = 0.125$ up to $\tau = 0.2$ in the top panel of Fig. 1.11(b) illustrate this phenomenon. One also notices from the bottom panel of Fig. 1.11(b) that at higher values of τ the dispersion curves become discontinuous and have bands of forbidden *ka* regions.

1.3.2.3 Stability of Phase-Locked States

So far we have only discussed the existence conditions for plane wave states of (1.44) in the parameter domain of the wave number, coupling strength, frequency, and time delay. We also need to know the stability of such states in order for them to be excited and sustained in the system. In this section we will carry out a linear stability analysis of the equilibrium phase-locked solutions discussed in the previous section. We let

$$Z_j(t) = \left[R_k e^{i\omega_k t} + u_j(t)\right] e^{i(jka)}, \tag{1.58}$$

where $k = 0, 1, \cdots, N-1$, substiute it in (1.44), and carry out an order by order analysis in the perturbation amplitude u_j. In the lowest order we recover the dispersion relation (1.51). In the next order, where we retain terms that are linear in the perturbation amplitude, we get

$$\begin{aligned}\frac{\partial u_j(t)}{\partial t} &= \left(1 + i\omega_0 - 2R_k^2 - 2K\right) u_j(t) - R_k^2 e^{2i\omega_k t}\bar{u}_j(t) \\ &+K\left[u_{j+1}(t-\tau)\, e^{ika} + u_{j-1}(t-\tau)\, e^{-ika}\right]\end{aligned} \tag{1.59}$$

and, taking its complex conjugate,

$$\begin{aligned}\frac{\partial \bar{u}_j(t)}{\partial t} &= \left(1 - i\omega_0 - 2R_k^2 - 2K\right)\bar{u}_j(t) - R_k^2 e^{-2i\omega_k t} u_j(t) \\ &\quad + K\left[\bar{u}_{j+1}(t-\tau)\, e^{-ika} + \bar{u}_{j-1}(t-\tau)\, e^{ika}\right].\end{aligned} \tag{1.60}$$

We next multiply (1.59) and (1.60) term by term by $e^{i(jqa)}$ and make use of the identities

$$u_{j\pm1}(t-\tau)\, e^{\pm ika} e^{i(jqa)} = u_{j\pm1}(t-\tau)\, e^{i(j\pm1)qa} e^{\pm i(k-q)a} \tag{1.61}$$

and

$$\bar{u}_{j\pm1}(t-\tau)\, e^{\pm ika} e^{i(jqa)} = \bar{u}_{j\pm1}(t-\tau)\, e^{i(j\pm1)qa} e^{\pm i(k+q)a}, \tag{1.62}$$

and finally sum over $j = 0, 1, 2, \cdots, N-1$. Introducing adjoint amplitudes $w_q(t)$ and $\tilde{w}_q(t)$ by the definitions

$$\left[w_q(t), \tilde{w}_q(t)\right] = \sum_{j=0}^{N-1} \left[u_j(t), \bar{u}_j(t)\right] e^{i(jqa)}, \tag{1.63}$$

we can arrive at the following set of coupled equations:

$$\begin{aligned}\frac{dw_q(t)}{dt} &= \left(1 + i\omega_0 - 2R_k^2 - 2K\right) w_q(t) - R_k^2 e^{2i\omega_k t}\tilde{w}_q(t) \\ &\quad + 2K\cos\left[(k-q)a\right] w_q(t-\tau)\end{aligned} \tag{1.64}$$

and

$$\begin{aligned}\frac{d\tilde{w}_q(t)}{dt} &= \left(1 - i\omega_0 - 2R_k^2 - 2K\right)\tilde{w}_q(t) - R_k^2 e^{-2i\omega_k t} w_q(t) \\ &\quad + 2K\cos\left[(k+q)a\right]\tilde{w}_q(t-\tau).\end{aligned} \tag{1.65}$$

Now assuming the solutions to be of the form

$$\left[w_q(t), \tilde{w}_q(t)\right] = \left[ce^{i\omega_k t}, \tilde{c}e^{-i\omega_k t}\right] e^{\lambda t}, \tag{1.66}$$

one can, after some straightforward algebra, obtain the following eigenvalue equation:

$$\lambda^2 + (a_1 + a_2)\lambda + (a_1 a_2 - R^4) = 0, \tag{1.67}$$

where

$$a_1 = 2R^2 - 1 + 2K - i(\omega_0 - \omega) - 2K\cos[(k-q)a]\mathrm{e}^{-(\lambda+i\omega)\tau}, \quad (1.68)$$

$$a_2 = 2R^2 - 1 + 2K + i(\omega_0 - \omega) - 2K\cos[(k+q)a]\mathrm{e}^{-(\lambda-i\omega)\tau}. \quad (1.69)$$

The perturbation wave numbers q are a discrete set that obey the relation

$$qa = m\frac{2\pi}{N}, \quad m = 0, 1, \ldots, N-1.$$

Thus, for any given plane wave pattern characterized by a given value of ka, one needs to examine the eigenvalues of (1.67) at each of the above permitted values of qa, which is a formidable task for any reasonably large value of N and one needs to carry out extensive numerical investigations. Some specific examples have been worked out in [35]. In general, time delay appears to expand the stability domain of plane wave states allowing for a richer spectrum of states to be sustained in the system as compared to the no-delay case. For example, the out of phase state (where each oscillator is π out of phase with its neighbor) which is always unstable in the absence of time delay can get stabilized for certain values of τ. A numerical simulation of such an out-of-phase state is shown in Fig. 1.11(c) where the level of the real part of Z_j is plotted as a function of the oscillator number j for $N = 50$ oscillators.

1.3.3 Non-Local Coupling

While global and local (nearest neighbor) coupling models have received much attention in the past, [1, 2, 39–41] there is now a growing interest in the collective dynamics of models with non-local couplings [42–48]. Non-local coupling implies a form of coupling in which the coupling extends over a wider domain than the local (nearest neighbor coupling) but with varying (usually diminishing) coupling strength. The coupling strength can fall off exponentially or in some cases even change sign with distance (for example, in a Mexican hat fashion). Non-local coupling can be relevant to a variety of applications such as in the modeling of Josephson junction arrays [49], chemical oscillators [47, 48, 50], neural networks for producing snail shell patterns, and ocular dominance stripes [51–53]. They can also arise in a large class of reaction diffusion systems under certain limiting assumptions for the diffusion strength and local kinetics such that the dynamics is governed by an equation which is a non-local generalization of the CGLE [50, 54]. Another interesting and unique feature of a non-locally coupled system is that it can sustain some unusual collective states in which the oscillators separate into two groups—one that is synchronized and phase-locked and the other desynchronized and incoherent [47]. Such a state of co-existence of coherence and incoherence does not occur in either globally or locally coupled systems and has been named as a ‘chimera’ state by Strogatz [55]. The nature and properties of this exotic collective

state as well as its potential applications are still not fully explored or understood and therefore continue to offer exciting future possibilities. In this section we will explore the effect of time delay on the collective states of a non-locally coupled system, where in addition to looking at the amplitude death and phase-locked states we will also discuss the novel 'chimera' state.

1.3.3.1 Non-Local Model Equations

We begin by first extending our set of model equations from the previous section to include non-local time-delayed coupling. Considering again a closed chain of N identical limit cycle oscillators, we can generalize (1.44) to the following form:

$$\frac{\partial Z_j}{\partial t} = (1 + i\omega_0) Z_j(t) - |Z_j(t)|^2 Z_j(t) + KQ_j(t), \tag{1.70}$$

where K is the coupling constant, $Z_j(t)$ are the complex amplitudes of the oscillators, $j = 0, 1, 2, \ldots, (N-1)$, and

$$Z_{j+nN}(t) = Z_j(t), \; n = 0, \pm 1, \pm 2, \ldots \tag{1.71}$$

The total coupling function acting on the jth oscillator, $Q_j(t)$, is given by

$$Q_j(t) = S_{e,o} \sum_{\{e,o\}} e^{-m\kappa a} \left\{ \left[Z_{j+m}(t - m\tau) - Z_j(t) \right] + \left[Z_{j-m}(t - m\tau) - Z_j(t) \right] \right\}, \tag{1.72}$$

where a is the distance and τ is the time delay between two adjacent oscillators, respectively. The labels e and o indicate cases in which, respectively, N is even and N is odd. The two cases must be treated separately. The total coupling function is a sum over m for pairwise couplings of oscillators and excludes self-coupling. If we compare (1.70) (keeping in mind (1.72)) with the model set of equations for the locally coupled system (1.44), we notice the following essential differences. The coupling strength K is now weighted by a factor $\exp(-m\kappa a)$ which is distance dependent and therefore makes the coupling from distant oscillators progressively weaker. The time delay dependence in the argument of each Z_j is likewise a function of $m\tau$ which implies that the amount of time a signal takes to arrive at a given oscillator location increases linearly as the distance it has to travel from another oscillator. Physically this amounts to assuming a constant signal velocity v in the system such that $\tau = a/v$. The exponentially decaying weight factor that we have chosen for this model can be replaced by other functions to change the nature of coupling, but we will restrict ourselves to this function as it has been used in some past calculations [45, 47, 48] that were done in the absence of delay and hence provides a convenient benchmark for assessing delay effects. The exponential damping coefficient κ provides a measure of the amount of non-locality in the coupling with $\kappa = 0$ being the global coupling limit. In order that the coupling amplitude be an exponential function of the distance between coupled oscillators, rather than a truncated exponential

function of that distance, it is necessary that the effective coupling range be less than half the length of the ring. If we denote the length of the ring by $2L$, then the minimum value of κ for which truncation does not occur is the value that yields the largest value of $\exp(-\kappa L)$ that can be considered negligible. It is convenient for this purpose to adopt the condition $\kappa L \geq 2\pi$, because $\exp(-2\pi) = 0.00187$. The choice $L = \pi$ is particularly convenient for the Fourier analysis of the discrete system because it yields the primitive basis set $e_k(m) = \exp(imka)$, where $a = (2\pi/N)$ and $m, k = 0, 1, 2, \ldots, (N-1)$. For other choices of L, k and a have different values, but ka is invariant with respect to the choice of L.

The quantity $S_{\{e,o\}}$ is a normalization factor. By assigning the value 1 to each coupling term, $\left[Z_{j\pm m}(t - m\tau) - Z_j(t)\right]$, and requiring that the value of the associated total coupling function is 1, we obtain

$$S_{\{e,o\}} = \left(2\sum_{\{e,o\}} e^{-m\kappa a}\right)^{-1}. \tag{1.73}$$

The correctness of this choice is demonstrated in the case that $N = 2$ and $\kappa = 0$, where one obtains (1.44) as intended. The form of the normalization factor makes it possible to express the total coupling function in the simplified form

$$Q_j(t) = S_{\{e,o\}} \sum_{\{e,o\}} e^{-m\kappa a}\left[Z_{j+m}(t - m\tau) + Z_{j-m}(t - m\tau)\right] - Z_j(t). \tag{1.74}$$

In the case in which N is even, the summation is

$$\sum_e = \sum_{m=1}^{\frac{1}{2}N}\left(1 - \frac{1}{2}\delta_{m,\frac{1}{2}N}\right). \tag{1.75}$$

The quantity in parentheses is introduced to account for the fact that the subscripts $j + \frac{1}{2}N$ and $j - \frac{1}{2}N$ denote the same oscillator.

In the case in which N is odd, the summation is

$$\sum_o = \sum_{m=1}^{\frac{1}{2}(N-1)}. \tag{1.76}$$

One obtains for S_e the result

$$S_e = \frac{1}{2}\left[\frac{1 - e^{-\kappa a}}{e^{-\kappa a} - \frac{1}{2}e^{-\frac{1}{2}N\kappa a} - \frac{1}{2}e^{-\left(\frac{1}{2}N+1\right)\kappa a}}\right]. \tag{1.77}$$

In the limit $\kappa \to 0$, one obtains $S_e = (N-1)^{-1}$. In that limit and for the case $N = 2$, one obtains the correct result, $S_e = 1$. One obtains for S_o the result

$$S_o = \frac{1}{2}\left[\frac{1 - e^{-\kappa a}}{e^{-\kappa a} - e^{-\frac{1}{2}(N+1)\kappa a}}\right]. \tag{1.78}$$

In the limit $\kappa \to 0$, one obtains $S_o = (N-1)^{-1}$.

It is interesting to also consider the continuum limit of (1.70), (1.71), and (1.72) in the spirit of what we did for the locally coupled system. This limit can be achieved by adopting the following procedure: We let the number of oscillators N increase without limit, i.e., $N \to \infty$, but keep the system length $2L$ unchanged. This implies that $a \to 0$ but $Na = 2L$. As before, the discrete variable that denotes the position of an oscillator, j, is replaced by the continuous variable x $(-L \le x < L)$, so that the discrete oscillator amplitude, $Z_j(t)$, becomes the continuous oscillator amplitude, $Z(x, t)$. The discrete variable that denotes the distance between coupled oscillators, m, is replaced by the continuous variable $0 \le y \le L$, so that the discrete total coupling function $Q_j(t)$ becomes the continuous total coupling function $Q(x, t)$. Consider first the normalization factors $S_{\{e,o\}}$. As the continuous limit is approached, it is necessary that the range of the non-local coupling be much greater than the distance between adjacent oscillators, i.e., that $\kappa a \ll 1$, which ensures that $\exp(-\kappa a) \approx 1 - \kappa a$. The condition $\kappa L \ge 2\pi$, which is necessary to guarantee that the form of the damping function is an exponential function, rather than a truncated exponential function, ensures that $\frac{1}{2}N\kappa a \ge 2\pi$, which in turn ensures that $\exp\left(-\frac{1}{2}N\kappa a\right) \ll 1$. Accordingly, we conclude that in the continuous limit $S_{\{e,o\}} = \frac{1}{2}\kappa a$. Assuming that the delay time between adjacent oscillators is proportional to the distance between them, we obtain the following relation between these quantities and σ, the reciprocal of the speed of propagation of delay coupling in the continuous case: $\sigma = \tau/a$. In the continuous limit, t_d, the earlier time at which a coupling signal originates from position $x \pm y$ to reach position x at time t is $t_d = t - \sigma y$. The correspondence between summation in the discrete case and integration in the continuous case is

$$\sum_{\{e,o\}} a \to \int_0^L dy.$$

The condition $\kappa L \ge 2\pi$ permits to replace the upper limit of integration, L, by ∞. Thus, we obtain as the continuous limit of (1.70), (1.71) and (1.72)] the set of equations

$$\frac{\partial}{\partial t} Z(x,t) = (1 + i\omega_0) Z - |Z|^2 Z + KQ(t), \tag{1.79}$$

$$Z(x + 2Ln, t) = Z(x,t) \quad n = 0, \pm 1, \pm 2, \ldots, \tag{1.80}$$

and

$$Q(x,t) = \int_0^\infty dy \frac{1}{2}\kappa e^{-\kappa y}\left[Z(x+y,\, t-\sigma y) + Z(x-y,\, t-\sigma y)\right] dy. \qquad (1.81)$$

Equation (1.79) is the non-local time-delayed generalization of the complex Ginzburg–Landau equation. One can also obtain a phase-reduced version of the above equation in the limit when the coupling between the oscillators is weak. We then let $Z = A\exp(i\phi(x,t))$ and treat the amplitude A to be a constant. In general the coupling constant K may be complex and can be written as $K(1+ia) = K'\exp(i\alpha)$ where a and α are real constants. Substituting for Z in (1.79) and separating the real and imaginary parts, we get from the imaginary part,

$$\frac{\partial\phi(x,t)}{\partial t} = \omega_0 + K'\int_{-L}^{L} dy\, G(x-x')\sin\left[\phi(x',\, t-\sigma \mid x-x' \mid) - \phi(x,\, t) + \alpha\right], \qquad (1.82)$$

where $\alpha = \tan^{-1}(a)$ and we have chosen the system length to be $2L$. In the absence of time delay (setting $\sigma = 0$) equations (1.79) and (1.82) have recently been studied by a number of authors [47, 48, 50] in the context of chimera states. We will return to these equation later in this section after we have discussed some aspects of the death state and phase-locked states in the discrete non-local system.

1.3.3.2 Amplitude Death in the Non-Local System

A linear perturbation analysis about the origin $Z_j = 0$, carried out for (1.70) in the manner described in the previous section, yields the following eigenvalue equation for N odd

$$\lambda_j = 1 + i\omega_0 - K + 2KS_o \sum_{m=1}^{\frac{1}{2}(N-1)} \cos\left[\frac{2\pi}{N}(j-1)m\right] e^{-m(\kappa a+\lambda_j\tau)}, \qquad (1.83)$$

and likewise for even N one can get

$$\lambda_j = 1 + i\omega_0 - K\left[1 + S_e e^{-N(\kappa a+\lambda_j\tau)/2}\cos(\pi(j-1))\right] + 2KS_e\sum_{m=1}^{N/2}\cos\left(\frac{2\pi}{N}(j-1)m\right)e^{-m(\kappa a+\lambda_j\tau)}. \qquad (1.84)$$

Notice the similarities and some essential differences between (1.83) (or (1.84)) and the individual factors of the eigenvalue equation (1.46) that we derived earlier for the locally coupled system. In addition to the weight factor $\exp(-\kappa a)$ we also see that there is a summation over all perturbation wave numbers $2\pi(j-1)/N$. One can therefore expect a more complex shape for the island structure compared to the two or at most four curves for the locally coupled system. The parameter κa

provides a measure of the degree of non-locality—a large κa corresponds to a highly localized interaction region and a small value of κa implies stronger non-locality. One can also expect therefore a dependence of the island complexity on the value of κa. These expectations are indeed borne out [36] when one constructs the stability islands in the $K-\tau$ parameter space by using the marginal stability curves of (1.83) or (1.84). For the odd N case the marginal curves are defined by the following two relations:

$$1-K+2KS_o\sum_{m=1}^{(N-1)/2}e^{-m\kappa a}\cos(m\tau\beta)\cos(\frac{2\pi}{N}(j-1)m)=0, \tag{1.85}$$

$$\omega_0+2KS_o\sum_{m=1}^{(N-1)/2}e^{-m\kappa a}\sin(m\tau\beta)\cos(\frac{2\pi}{N}(j-1)m)=\beta, \tag{1.86}$$

where $\beta = \mathrm{Im}(\lambda_j)$. To construct the marginal curves, i.e., to derive a relation between K and τ one needs to eliminate β from the above two equations. This is difficult to do analytically but can be accomplished numerically by rewriting the above equations in the following parametric form:

$$K=\frac{1}{1-2S_o\sum_{m=1}^{(N-1)/2}e^{-m\kappa a}\cos(mx)\cos(my)}, \tag{1.87}$$

$$\tau=\frac{x}{\omega_0+2K(x)S_o\sum_{m=1}^{(N-1)/2}e^{-m\kappa a}\sin(mx)\cos(my)}, \tag{1.88}$$

where $x=\beta\tau$ and $y=\frac{2\pi}{N}(j-1)$. For a given value of κa and N, the idea is to evaluate K and τ numerically over a range of x values, e.g. $(-2\pi,0)$, for a particular value of y and thereby eliminate β. The evaluation is repeated for each value of y. The stable region bounded by these curves then constitutes the death island. In Fig. 1.12(a) we have plotted the lower portions of the islands for two cases, namely $\kappa a=1$, for which the non-locality is strong, and $\kappa a=3$, which is close to being a locally coupled system. As can be seen the lower boundary of the strongly coupled case is quite complex and is made up of portions of several marginal stability curves arising from different mode number perturbations. By contrast, for the weakly non-local case the island region lies between just two curves as shown in Fig. 1.12(b). Another important difference from the local coupling case is that the island size is no longer invariant for even N but changes as a function of N.

1.3.3.3 Plane Wave States and their Stability

As in the case of the nearest neighbor coupled system, a non-locally coupled system can also sustain plane wave solutions. The plane wave form of the complex amplitude of the jth oscillator, including a perturbation of order ϵ, is

$$Z_j(t)=\left[1+\epsilon a_j(t)\right]Z_j^0(t), \tag{1.89}$$

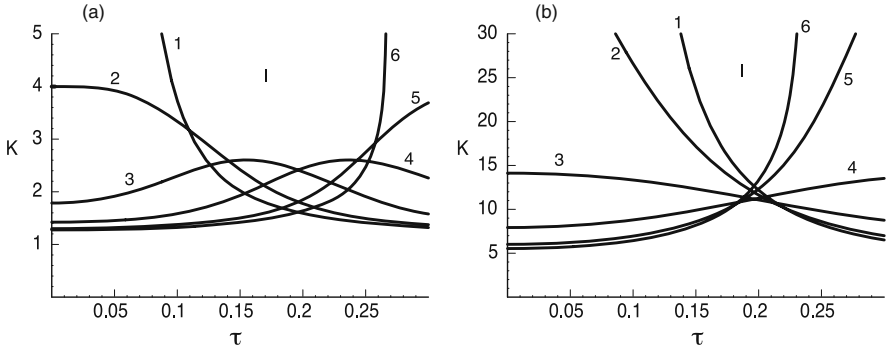

Fig. 1.12 (**a**) The lower portion of a death island for strong non-locality $\kappa a = 1, N = 10$, for small K. All the perturbation modes participate in defining the boundary where the curves are labeled by $j = 1, 2, 3...$ (**b**) A similar plot for weak non-locality, $\kappa a = 3, N = 10$ where only two perturbation modes $j = 1$ and $j = 6$ are seen to define the boundary

where

$$Z_j^0(t) = \mathcal{R}_k e^{i(jka+\omega_k t)}, \tag{1.90}$$

$k = 0, 1, 2, \ldots, (N-1)$, $\mathcal{R}_k^2$ is required to be positive, and $a_j(t)$ are the complex amplitudes of the perturbation, which satisfy the periodicity conditions $a_{j+nN}(t) = a_j(t)$, $n = 0, \pm 1, \pm 2, \ldots$. In general, ω_k is complex, but for plane wave equilibria ω_k is required to be real. The quantities $\mathcal{R}_k^2$ and ω_k are determined simultaneously by solution of a complex dispersion relation obtained at $O\left(\epsilon^0\right)$ of a perturbation expansion in ϵ. A system of evolution equations for the set of functions $a_j(t)$, from which the linear stability of the equilibria is determined, is obtained at $O(\epsilon)$ of the perturbation expansion. The dispersion relation for plane wave solutions of (1.70) is given by the pair of equations

$$\omega_k = \omega_0 + K\Im\left\{\tilde{Q}\right\} \tag{1.91}$$

and

$$\mathcal{R}_k^2 = 1 + K\Re\left\{\tilde{Q}\right\}, \tag{1.92}$$

where

$$\tilde{Q} = S_{\{e,o\}} \sum_{\{e,o\}} e^{-m(\kappa a + i\omega_k \tau)} \left(e^{imka} + e^{-imka}\right) - 1 \tag{1.93}$$

and the symbols $\Re\{\}$, $\Im\{\}$ stand for the real and imaginary parts of the quantity within the braces. For a given value of k, one determines numerically the values of ω_k that satisfy (1.91). For each set of values of k and ω_k, one then determines

from (1.92) the value of $\mathcal{R}_k^2$, which, for an acceptable set of values of k and ω_k, is required to be positive. In the case of vanishing time delay, the quantities $\tilde{Q}$ are independent of ω_k, a given value of k determines a single value of ω_k, and the solution of (1.92) and (1.91) for ω_k and $\mathcal{R}_k^2$ is considerably simplified. Having determined a set of equilibrium states $(\omega_k, \mathcal{R}_k)$, one needs to next determine their stability from an eigenvalue analysis. The derivation of such an eigenvalue equation is quite straightforward, if somewhat tedious, and is along the lines of the method followed for the nearest neighbor case. The analysis of such an equation for large N is however quite challenging even numerically and remains an open problem at the present time.

1.3.3.4 Time-Delayed Chimera States

Non-locally coupled oscillator systems can exhibit a remarkable class of patterns called *chimeras*, in which identical limit cycle oscillators separate sharply into two domains, one synchronized and phase-locked and the other desynchronized and drifting [47]. This peculiar mode, in which coherence and incoherence co-exist at the same time in a system of oscillators, was first noticed by Kuramoto and his coworkers [47, 48, 50] in their simulations of the complex Ginzburg–Landau equation (CGLE) with non-local coupling and was later named a *chimera* state by Abrams and Strogatz [55]. In Fig. 1.13(a) we show a typical plot of the chimera state in the absence of delay obtained from a numerical solution of (1.82) with $\sigma = 0$. One clearly sees two distinct regions—a central region where the phases of the oscillators are locked to each other and an outer region where they are randomly distributed. The central portion drifts with a certain fixed velocity while the incoherent part has no fixed velocity. A chimera is a stationary stable pattern that co-exists with a fully phase-locked coherent state and occurs in a limited parameter

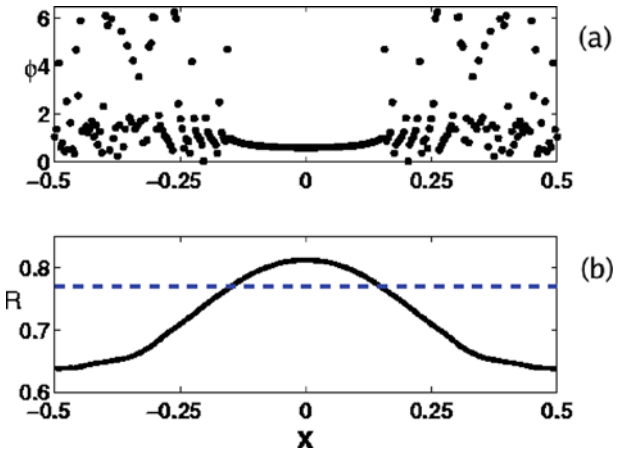

Fig. 1.13 Phase pattern for a typical chimera state. Here $K' = 1$, $\kappa = 4.0$, $\alpha = 1.45$, $\omega = 0$, and N = 257

regime defined by the coupling strength K' and the tuning parameter α. Access to such a state is also dependent on initial conditions and Kuramoto et al. [47] took special precautions to obtain such solutions numerically. Chimera solutions exist for both the CGLE and for the reduced phase-only version of the equation. For convenience we rewrite the phase-reduced NDCGL equation (1.82) once again here and set $K' = 1$ and drop the subscript on ω.

$$\frac{\partial}{\partial t}\phi(x,t) = \omega - \int_{-L}^{L} G(x-x')\sin\left[\phi(x,t) - \phi(x', t-\tau_{x,x'}) + \alpha\right] dx'. \qquad (1.94)$$

The kernel $G(x - x')$ provides a non-local coupling among the oscillators over a finite spatial range of the order of κ^{-1}, which is chosen to be less than the system size. The coupling is time delayed through the argument of the sinusoidal interaction function, namely, the phase difference between two oscillators located at x and x' is calculated by taking into account the temporal delay for the interaction signal to travel the intervening geodesic (i.e., shortest) distance determined as $d_{x,x'} = \min\{|x - x'|, 2L - |x - x'|\}$. The time delay term is therefore taken to be of the form $\tau_{x,x'} = d_{x,x'}/v$ where v is the signal propagation speed.

The question we now ask is whether (1.94) has a chimera solution in the presence of finite time delay and what it looks like. This problem was addressed in [37] exploring both numerical solutions of (1.94) and some analytical insights obtained from the behavior of the order parameter. We first discuss the numerical results obtained by using the discretized version of (1.94) and employing a large number of oscillators (typically 257) for the simulation. The set of system parameters chosen for the simulations were $2L = 1.0$, $\alpha = 0.9$, $k^{-1} = 0.25$, $\omega = 1.1$, and $v = 0.09765625$ corresponding to a maximum delay time ($\tau_{\max}$) in the system of 5.12. Initially all the oscillators were given uniformly random phases (mirror symmetric) between 0 and 2π, and the equations were evolved long enough to get a time-stationary solution. Figure 1.14 provides a comprehensive summary of the evolution and final state of the time-delayed chimera. Panels (a) and (b) show a space–time plot of the simulation in the early stages of evolution (starting from random initial phases) and in the final stages of the formation of a *clustered chimera* state, respectively. Panel (c) shows a snapshot of the spatial distribution of the phases in the final stationary state. We see four coherent regions interspersed by incoherence and also find that the adjacent coherent regions are π out of phase with each other. Panel (d) is a blowup of the region between $x = -0.5$ and $x = -0.25$ giving an enlarged view of an incoherent region and portions of the adjacent coherent regions.

To gain a better understanding of the nature of this pattern and of the dynamics of its formation, it is instructive to adopt a generalized mean field approach and try to examine the behavior of an averaged quantity like an order parameter of the system. Such an approach and formalism was developed by Kuramoto and Battogtokh [47] to understand the formation of the non-delayed chimera state. For this, we first rewrite (1.94) in terms of a relative phase θ given by

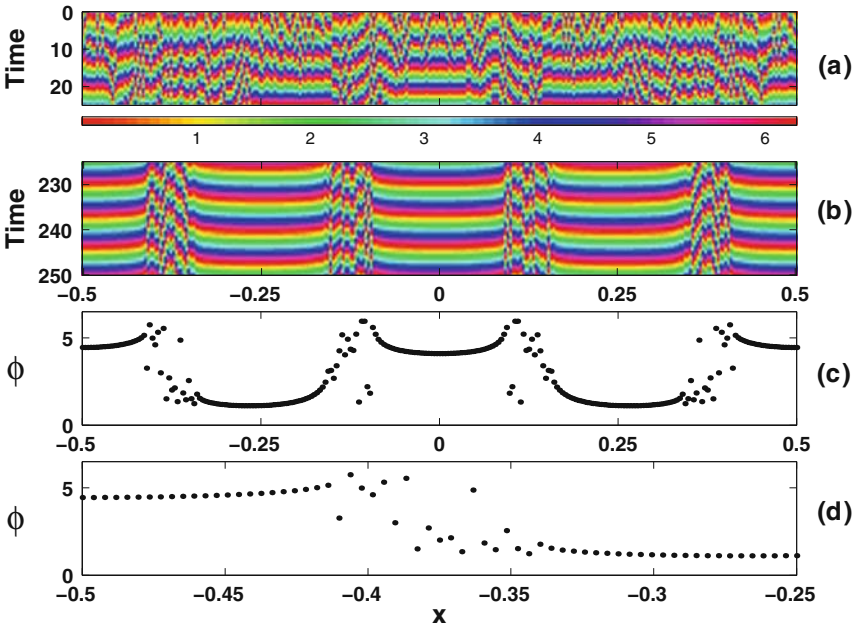

Fig. 1.14 (**a**) The space–time plot of the oscillator phases ϕ for the parameters $2L = 1.0$, $\kappa = 4.0$, $1/v = 10.24$, $\omega = 1.1$, and $\alpha = 0.9$ in the early stages of evolution from a random set of initial phases. Panel (**b**) shows a later time evolution and panel (**c**) gives a snapshot of the final stationary state. Panel (**d**) is a blowup of the region between $x = -0.5$ and $x = -0.25$ giving an enlarged view of an incoherent region and portions of the adjacent coherent regions

$$\theta(x,t) = \phi(x,t) - \Omega t, \tag{1.95}$$

where Ω represents a rotating frame in which the dynamics simplifies as much as possible and is the constant drift frequency of the phase-locked portions. In terms of θ (1.94) becomes

$$\frac{\partial}{\partial t}\theta(x,t) = \omega - \Omega - \int_{-L}^{L} G(x-x')\sin\left[\theta(x,t) - \theta(x',t-\tau_{x,x'}) + \alpha + \Omega\tau_{x,x'}\right]dx'. \tag{1.96}$$

Following Kuramoto's approach [47], we now define a complex order parameter $Re^{i\Theta}$, in a manner analogous to what we had done for a globally coupled system in Sect. 1.3.1, as,

$$R(x,t)e^{i\Theta(x,t)} = \int_{-L}^{L} G(x-x')e^{i[\theta(x',t-\tau_{x,x'}) - \Omega\tau_{x,x'}]}\,dx'. \tag{1.97}$$

The above order parameter differs from the usual definition for globally coupled systems in a number of significant ways: The spatial average of $e^{i\theta}$ is now weighted by the coupling kernel $G(x-x')$, the phase θ is evaluated in a time-delayed fashion,

and the factor $e^{-i\Omega\tau_{x,x'}}$ adds a complex phase to the kernel $G(x-x')$. The latter two features provide a further generalization of Kuramoto's analysis carried out for a non-delayed system [47, 48, 55, 56].

In terms of R and Θ, (1.94) can be rewritten as

$$\frac{\partial}{\partial t}\theta(x,t) = \Delta - R(x,t)\sin\left[\theta(x,t) - \Theta(x,t) + \alpha\right], \tag{1.98}$$

where $\Delta = \omega - \Omega$. Equation (1.98) is in the form of a single-phase oscillator equation driven by a force term which in this case is the mean field force. To obtain a stationary pattern (in a statistical sense) we require that R and Θ depend only on space and be independent of time. Under such a circumstance the oscillator population can be divided into two classes: those which are located such that $R(x) > |\Delta|$ can approach a fixed point solution ($\partial\theta(x,t)/\partial t = 0$) and the other oscillators that have $R(x) < |\Delta|$ would not be able to attain such an equilibrium solution. The oscillators approaching a fixed point in the rotating frame would have phase coherent oscillations at frequency Ω in the original frame whereas the other set of oscillators would drift around the phase circle and form the incoherent part.

One can easily solve (1.98) for the motion of the oscillator at each x, subject to the assumed time-independent values of $R(x)$ and $\Theta(x)$. The oscillators with $R(x) \geq |\Delta|$ asymptotically approach a stable fixed point θ^*, defined implicitly by

$$\Delta = R(x)\sin\left[\theta^* - \Theta(x) + \alpha\right]. \tag{1.99}$$

The fact that they approach a fixed point in the rotating frame implies that they are phase-locked at frequency Ω in the original frame. On the other hand, the oscillators with $R(x) < |\Delta|$ drift around the phase circle monotonically. To be consistent with the assumed stationarity of the solution, these oscillators must distribute themselves according to an invariant probability density $\rho(\theta)$. And for the density to be invariant, the probability of finding an oscillator near a given value of θ must be inversely proportional to the velocity there. From (1.98), this condition becomes

$$\rho(\theta) = \frac{\sqrt{\Delta^2 - R^2}}{2\pi\left|\Delta - R\sin\left(\theta - \Theta + \alpha\right)\right|}, \tag{1.100}$$

where the normalization constant has been chosen such that $\int_{-\pi}^{\pi}\rho(\theta)\,d\theta = 1$ and R, Θ, and θ are functions of x.

The resulting motions of both the locked and the drifting oscillators must be consistent with the assumed time-independent values of $R(x)$ and $\Theta(x)$. To calculate the contribution that the locked oscillators make to the order parameter (1.97), we note that

$$\sin(\theta^* - \Theta + \alpha) = \frac{\Delta}{R}, \tag{1.101}$$

$$\cos(\theta^* - \Theta + \alpha) = \pm\frac{\sqrt{R^2 - \Delta^2}}{R} \tag{1.102}$$

for any fixed point of (1.98). Taking plus sign for the stable fixed point, one can write

$$e^{i(\theta^* - \Theta + \alpha)} = \frac{\sqrt{R^2 - \Delta^2} + i\Delta}{R} \tag{1.103}$$

which implies that the locked oscillators contribute

$$\int dx' G(x - x') e^{i\theta^*(x')} = e^{-i\alpha} \int dx' G(x - x') e^{i[\Theta(x') - \Omega\tau_{x,x'}]} \left(\frac{\sqrt{R^2 - \Delta^2} + i\Delta}{R} \right) \tag{1.104}$$

to the order parameter (1.97). Here the integral is taken over the portion of the domain where $R(x') \geq \Delta$.

Next, to calculate the contribution from the drifting oscillators, following the prescription provided by Kuramoto [47, 48] for the undelayed case, we replace $e^{i\theta(x')}$ in (1.97) with its statistical average $\int_{-\pi}^{\pi} e^{i\theta}\rho(\theta)\,d\theta$. Using (1.100) and contour integration, one obtains

$$\int_{-\pi}^{\pi} e^{i\theta}\rho(\theta)d\theta = \frac{i}{R}\left(\Delta - \sqrt{\Delta^2 - R^2}\right). \tag{1.105}$$

The contribution of the drifting oscillators to the order parameter can therefore be written as

$$\int dx' G(x - x') e^{-i\Omega\tau_{x,x'}} \int_{-\pi}^{\pi} e^{i\theta}\rho(\theta)\,d\theta = ie^{-i\alpha} \int dx' G(x - x') \\ e^{i[\Theta(x') - \Omega\tau_{x,x'}]} \left(\frac{\Delta - \sqrt{\Delta^2 - R^2(x')}}{R(x')} \right), \tag{1.106}$$

where now the integral is over the complementary portion of the domain where $R(x') < |\Delta|$. We substitute these solutions of (1.98) for the two classes of oscillators into the integrand on the right-hand side of (1.97) and obtain the following functional self-consistency condition:

$$R(x)e^{i\Theta(x)} = e^{i\beta} \int_{-L}^{L} G(x - x') e^{i[\Theta(x') - \Omega\tau_{x,x'}]} \left(\frac{\Delta - \sqrt{\Delta^2 - R^2(x')}}{R(x')} \right) dx', \tag{1.107}$$

where $\beta = \pi/2 - \alpha$. For a chimera state to exist, R, Θ, and Δ must satisfy the above self-consistency condition. Note that we have three unknowns, and condition

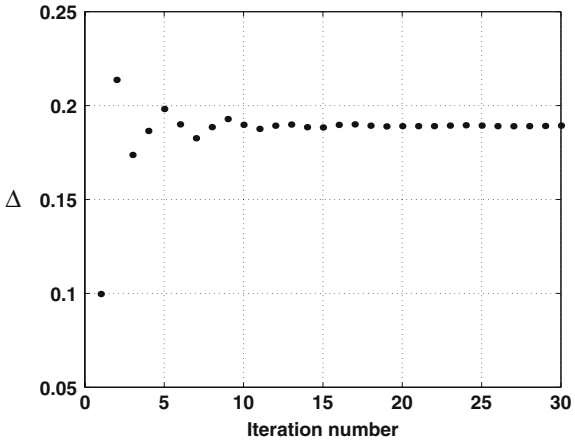

Fig. 1.15 Variation of Δ with the iteration number showing a rapid convergence in the numerical solution of the self-consistency equation (1.107). The system parameters are identical to those used in the direct solution of (1.94)

(1.107) provides only two equations when we separate its real and imaginary parts. A third condition can be obtained by exploiting the fact that the equation is invariant under any rigid rotation $\Theta(x) \rightarrow \Theta(x) + \Theta_0$. We can therefore specify the value of $\Theta(x)$ at any arbitrary chosen point, e.g., $\Theta(L) = 0$. In [37] (1.107) was solved numerically by following a three-step iterative procedure consisting of the following steps: Arbitrary but well-behaved initial guess functions were chosen for $R(x)$ and $\Theta(x)$ and the condition $\Theta(L) = 0$ was used in one of the equations of (1.107) to obtain a value for Δ. The initial profiles and the Δ value so obtained were then used to evaluate the right-hand side of (1.107) to generate new profiles for R and Θ. These were next used to generate a new value of Δ and the procedure was repeated until a convergence in the value of Δ and the functions R and Θ was obtained.

Figure 1.15 shows the rapid and excellent convergence in Δ to a unique value of $\Delta = 0.189$ for the solution of (1.107) with system parameters chosen identical to the ones that were used to obtain a clustered chimera state by a direct solution of (1.94). The converged spatial profiles of the order parameter (R and Θ) are shown in Fig. 1.16 and the converged value of Δ is marked in the upper panel by the horizontal line. The amplitude of the order parameter (R) shows a periodic spatial modulation—peaking at four symmetrically placed spatial locations. The corresponding phases of the order parameter are seen to be in anti-phase for adjacent peaks in R. In between the peaks R is seen to dip to very small values at certain locations such that $R(x) < |\Delta|$ which should correspond to the incoherent drifting parts of the chimera. To better appreciate the agreement between the direct solutions of (1.94) and the mean field solutions of (1.107) the results are plotted together in Fig. 1.17. As is clearly seen the measured order parameter (R and Θ) and Δ from the direct simulations of (1.94) match well with the results of solving (1.107). The spatial profile of the phases (ϕ) of the oscillators as obtained from the direct simulation of (1.94) is shown in the top panel of Fig. 1.17. One finds four coherent regions interspersed by incoherence as expected from the results of solving (1.107).

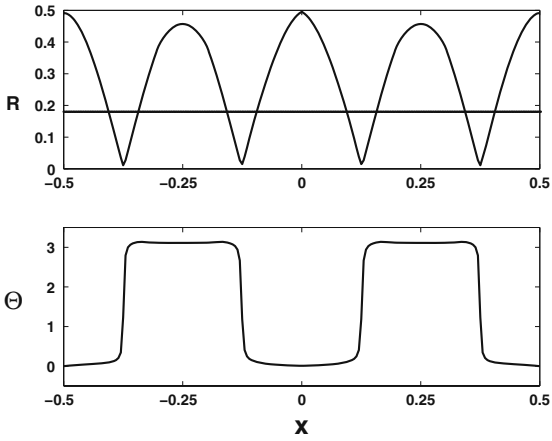

Fig. 1.16 Spatial profiles of the amplitude R and the phase Θ of the order parameter obtained by solving the self-consistency equation (1.107) by an iterative scheme. The horizontal line in the upper panel marks the converged value $\Delta = 0.189$

Also note that for the no-delay case there is only one peak of the order parameter as shown in Fig. 1.13(b).

It is appropriate at this juncture to point out some other general features of the clustered chimera states. Figures 1.16 and 1.17 show that both R and Θ are mirror symmetric (i.e., $R(x) = R(-x), \Theta(x) = \Theta(-x)$), a property that the original phase equation (1.94) also possesses. Equation (1.94) is also invariant under the

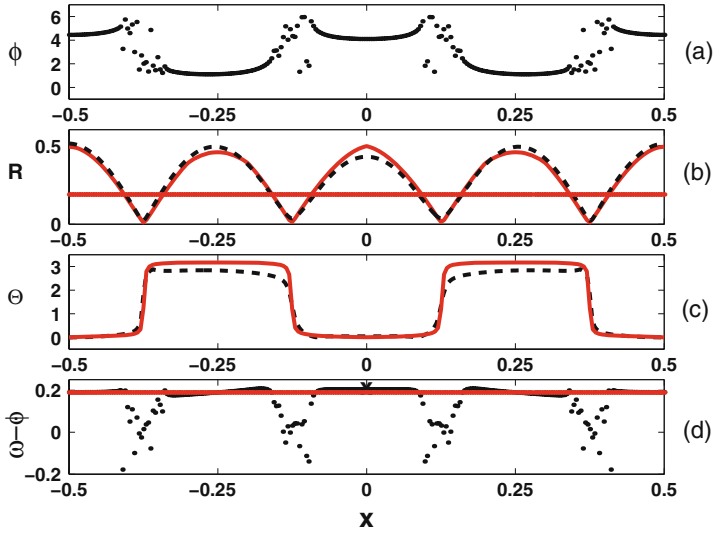

Fig. 1.17 (**a**) The phase pattern for a clustered chimera state as obtained by direct simulation of (1.94). The measured spatial profiles of the order parameter (R and Θ) from these simulations are shown in panels (**b**) and (**c**) as *dashed curves* and compared with the solutions from the self-consistency Equation (1.107) shown as *solid curves*. (**d**) $\omega - \dot{\phi}$ for the oscillators from a direct simulation of (1.94). The horizontal lines in (**b**) and (**d**) mark the converged value of $\Delta = 0.189$

transformation ($\phi(x,t) \rightarrow -\phi(x,t)$, $\omega \rightarrow -\omega$, $\alpha \rightarrow -\alpha$) and can have solutions with such a symmetry as well, namely, traveling wave solutions given by $\phi(x,t) = \Omega t + \pi q x/L$. In the numerical simulations with a change of the initial conditions keeping the same system parameters, one can get traveling wave solutions. For the non-delayed chimera case the co-existent stable state is that of a uniformly coherent state. The corresponding co-existent state in the time-delayed case is a traveling wave. In fact, there seems to be a clear correspondence between the number of clusters of the observed chimera state and the wave number q of the co-existent traveling wave solution. For the four-cluster chimera of Fig. 1.16 the co-existent traveling wave has $q = 2$ and similar results were observed in [37] for six-cluster ($q = 3$) and eight-cluster ($q = 4$) chimera solutions.

To summarize, we see that chimera type solutions do exist in a time-delayed system of non-locally coupled identical phase oscillators and that time delay leads to novel clustered states with a number of spatially disconnected regions of coherence with intervening regions of incoherence. The adjacent coherent regions of this clustered chimera state are found to be in anti-phase relation with respect to each other. These results are also well understood in terms of the behavior of a generalized order parameter for the system.

1.4 Summary and Perspectives

In the preceding sections we have shown how time delay can have subtle and sometimes profound effects on the collective dynamics of a coupled oscillator system. Various scenarios have been considered—starting from a simple two-oscillator model to a system of a large number of oscillators coupled in various ways. Time delay is introduced in the coupling mechanism and is seen to affect the existence, stability, and nature of the various collective states. Most of the basic effects associated with time delay are well demonstrated by the simple two-oscillator model. These include the phenomenon of time delay-induced amplitude death of identical oscillators, the existence of higher frequency oscillatory states, multistability and the co-existence of in-phase and anti-phase states, and multi-connectedness of death islands. For large N systems and in the presence of spatial dependence of the coupling mechanism, one has a wider variety of collective states such as traveling waves and the peculiar chimera state. Time delay affects the domain of existence of traveling waves as well as significantly altering their stability properties. The chimera state acquires a spatial modulation in the presence of time delay whose periodicity is closely linked to the co-existent stable traveling wave that the system can support. While the principal features of time-delayed dynamics, as displayed by the minimal model, are seen to be present in the N-oscillator models, their detailed analysis gets progressively difficult with increasing complexities of the coupling mechanisms and coupling topologies. Thus, as we found for the case of traveling wave states in nearest neighbor coupled as well as in non-locally coupled systems, the dispersion relations for their equilibrium states are extremely complicated and

demand extensive numerical analysis. The eigenvalue equations for linear stability are even more complex and do not permit an easy determination of the stability domains in parameter space. Due to the transcendental nature of these equations, there is some debate about the practical feasibility of applying some of the standard stability analysis techniques and this is very much an open area of research for future investigations. We would also like to remark here that in our analysis we have restricted ourselves to a very simple model of time delay—either a single fixed discrete delay or a discrete set of delays for the non-local case. Alternative representations of time delay are possible, such as the one used by Atay [57] who showed that the parameter space of amplitude death for the coupled oscillator is enhanced when the oscillators are connected with time delays distributed over an interval rather than concentrated at a point. Distributed delays provide for a more realistic model for the description of larger physical systems where the delay parameter can be space- or time-dependent or in biological systems where memory effects are important. Another limitation of our treatment has been the adherence to a single and simple kind of a collective model—namely an array of Stuart–Landau oscillators. Networks of pulse coupled oscillators (also known as integrate and fire models) have been widely explored in the context of neuronal studies and provide a more realistic description of such systems. Such systems are also found to be quite sensitive to the presence of time-delayed coupling, e.g., in enhancing the onset of neural synchrony [58]. Another area that we have not discussed in this chapter is the response of the oscillator system to an external time-delayed stimulus. This is an active area of research today with important applications in neuroscience and control of neural disorders. The basic idea here is again the influence of a time-delayed feedback in enhancing or suppressing self-synchronization in an assembly of oscillators. We have also restricted ourselves to the study of time delay effects on stationary (equilibrium) states of the system. Their influence can extend to time-dependent states as well as chaotic dynamics, Hopf oscillations, etc. In fact, the nature of transition between chaotic and unsynchronized states is to date a poorly understood and open problem in the study of coupled oscillator systems. Time delay effects, which provide a sensitive probe by its subtle influence on the behavior of the order parameter, can prove useful in the further exploration of this problem [33].

References

1. A. T. Winfree. *The Geometry of Biological Time*. Springer-Verlag, New York, 1980.
2. Y. Kuramoto. *Chemical Oscillations, Waves and Turbulence*. Springer, Berlin, 1984.
3. S. H. Strogatz. From Kuramoto to Crawford: exploring the onset of synchronization in populations of coupled oscillators. *Physica D*, 143:1–20, 2000. and references therein.
4. K. Satoh. Computer experiment on the cooperative behavior of network of interacting nonlinear oscillators. *J. Phys. Soc. Japan*, 58:2010–2021, 1989.
5. G. B. Ermentrout. Oscillator death in populations of "all to all" coupled nonlinear oscillators. *Physica D*, 41:219–231, 1990.
6. A. A. Brailove and P. S. Linsay. An experimental study of a population of relaxation oscillators with a phase-repelling mean-field coupling. *Int. J. Bifurcation Chaos*, 6:1211–1253, 1996.

7. P. Hadley, M. R. Beasley, and K. Wiesenfeld. Phase locking of Josephson-junction series arrays. *Phys. Rev. B*, 38:8712–8719, 1988.
8. K. Wiesenfeld, P. Colet, and S. H. Strogatz. Synchronization transitions in a disordered Josephson series array. *Phys. Rev. Lett.*, 76:404–407, 1996.
9. P. M. Varangis, A. Gavrielides, T. Erneux, V. Kovanis, and L. F. Lester. Frequency entrainment in optically injected semiconductor lasers. *Phys. Rev. Lett.*, 78:2353–2356, 1997.
10. A. Hohl, A. Gavrielides, T. Erneux, and V. Kovanis. Localized synchronization in two coupled nonidentical semiconductor lasers. *Phys. Rev. Lett.*, 78:4745–4748, 1997.
11. G. Grüner and A. Zettl. Charge-density wave conduction – a novel collective transport phenomenon in solids. *Phys. Rep.*, 119:117–232, 1985.
12. J. Benford, H. Sze, W. Woo, R. R. Smith, and B. Harteneck. Phase locking of relativistic magnetrons. *Phys. Rev. Lett.*, 62:969–971, 1989.
13. I. Schreiber and M. Marek. Strange attractors in coupled reaction diffusion cells. *Physica*, 5D:258–272, 1982.
14. M. F. Crowley and I. R. Epstein. Experimental and theoretical studies of a coupled chemical oscillator: Phase death, multistability, and in-phase and out-of-phase entrainment. *J. Phys. Chem.*, 93:2496–2502, 1989.
15. M. Dolnik and I. R. Epstein. Coupled chaotic chemical oscillators. *Phys. Rev. E*, 54:3361–3368, 1996.
16. M. Kawato and R. Suzuki. Two coupled neural oscillators as a model of the circadian pacemaker. *J. Theor. Biol.*, 86:547–575, 1980.
17. Y. Kuramoto. Cooperative dynamics of oscillator community. *Prog. Theor. Phys. Suppl.*, 79:223–240, 1984.
18. H. Daido. Intrinsic fluctuations and a phase transition in a class of large populations of interacting oscillators. *J. Stat. Phys.*, 60:753–800, 1990.
19. S. Strogatz. *Sync: The Emerging Science of Spontaneous Order*. Hyperion, New York, 2003.
20. Y. Aizawa. Synergetic approach to the phenomena of mode-locking in nonlinear systems. *Prog. Theor. Phys.*, 56:703–716, 1976.
21. M. Shiino and M. Frankowicz. Synchronization of infinitely many coupled limit-cycle oscillators. *Phys. Lett. A*, 136:103–108, 1989.
22. M. Poliashenko and S. R. McKay. Chaos due to homoclinic orbits in two coupled oscillators with nonisochronism. *Phys. Rev. A*, 46:5271–5274, 1992.
23. J. L. Rogers and L. T. Wille. Phase transitions in nonlinear oscillator chains. *Phys. Rev. E*, 54:R2193–R2196, 1996.
24. D. G. Aronson, G. B. Ermentrout, and N. Kopell. Amplitude response of coupled oscillators. *Physica D*, 41:403–449, 1990.
25. R. E. Mirollo and S. H. Strogatz. Amplitude death in an array of limit-cycle oscillators. *J. Stat. Phys.*, 60:245–262, 1990.
26. K. Bar-Eli. On the stability of coupled chemical oscillators. *Physica D*, 14:242–252, 1985.
27. P. C. Matthews, R. E. Mirollo, and S. H. Strogatz. Dynamics of a large system of coupled nonlinear oscillators. *Physica D*, 52:293–331, 1991.
28. H. G. Schuster and P. Wagner. Mutual entrainment of two limit cycle oscillators with time delayed coupling. *Prog. Theor. Phys.*, 81:939–945, 1989.
29. E. Niebur, H. G. Schuster, and D. Kammen. Collective frequencies and metastability in networks of limit-cycle oscillators with time delay. *Phys. Rev. Lett.*, 67:2753–2756, 1991.
30. Y. Nakamura, F. Tominaga, and T. Munakata. Clustering behavior of time-delayed nearest-neighbor coupled oscillators. *Phys. Rev. E*, 49:4849–4856, 1994.
31. S. Kim, S. H. Park, and C. S. Ryu. Multistability in coupled oscillator systems with time delay. *Phys. Rev. Lett.*, 79:2911–2914, 1997.
32. D. V. Ramana Reddy, A. Sen, and G. L. Johnston. Time delay induced death in coupled limit cycle oscillators. *Phys. Rev. Lett.*, 80:5109–5112, 1998.
33. D. V. Ramana Reddy, A. Sen, and G. L. Johnston. Time delay effects on coupled limit cycle oscillators at Hopf bifurcation. *Physica D*, 129:15–34, 1999.

34. D. V. Ramana Reddy, A. Sen, and G. L. Johnston. Experimental evidence of time-delay induced death in coupled limit-cycle-oscillators. *Phys. Rev. Lett.*, 85:3381–3384, 2000.
35. R. Dodla, A. Sen, and G. L. Johnston. Phase-locked patterns and amplitude death in a ring of delay-coupled limit cycle oscillators. *Phys. Rev. E*, 69:056217, 2004.
36. M. P. Mehta, A. Sen, and G. L. Johnston. Amplitude death states of a ring of nonlocally-coupled limit cycle oscillators with time delay. *Proceedings of the National Conference on Nonlinear Systems and Dynamics*, Chennai, Feb.5-8, 2006, 2006.
37. G. C. Sethia, A. Sen, and F. M. Atay. Clustered chimera states in delay-coupled oscillator systems. *Phys. Rev. Lett.*, 100:144102, 2008.
38. P. C. Matthews and S. H. Strogatz. Phase diagram for the collective behavior of limit cycle oscillators. *Phys. Rev. Lett.*, 65:1701–1704, 1990.
39. S. Peles and K. Wiesenfeld. Synchronization law for a van der Pol array. *Phys. Rev. E*, 68:026220, 2003.
40. L. L. Bonilla, C. J. Perez Vicente, F. Ritort, and J. Soler. Exactly solvable phase oscillator models with synchronization dynamics. *Phys. Rev. Lett.*, 81:3643–3646, 1998.
41. H. Daido. Multibranch entrainment and scaling in large populations of coupled oscillators. *Phys. Rev. Lett.*, 77:1406–1409, 1996.
42. G.B. Ermentrout. The behavior of rings of coupled oscillators. *J. Math. Biol.*, 23:55–74, 1985.
43. P. C. Bressloff, S. Coombes, and B. de Souza. Dynamics of a ring of pulse-coupled oscillators: Group theoretic approach. *Phys. Rev. Lett.*, 79:2791–2794, 1997.
44. M. Barahona and L.M. Pecora. Synchronization in small-world systems. *Phys. Rev. Lett.*, 89:054101, 2002.
45. Y. Kuramoto. Scaling behavior of oscillators with non-local interaction. *Prog. Theor. Phys.*, 94:321–330, 1995.
46. Y. Kuramoto and H. Nakao. Origin of power-law spatial correlations in distributed oscillators and maps with nonlocal coupling. *Phys. Rev. Lett.*, 76:4352–4355, 1996.
47. Y. Kuramoto and D. Battogtokh. Coexistence of coherence and incoherence in nonlocally coupled phase oscillators. *Nonlinear Phenomena in Complex Systems*, 5:380–385, 2002.
48. Y. Kuramoto. *Nonlinear Dynamics and Chaos:Where Do We Go from Here?*, p 209. Institute of Physics, Bristol, UK, 2003.
49. J. R. Phillips, H. S. J. van der Zant, J. White, and T. P. Orlando. Influence of induced magnetic-fields on the static properties of josephson-junction arrays. *Phys. Rev. B*, 47:5219–5229, 1993.
50. S. I. Shima and Y. Kuramoto. Rotating spiral waves with phase-randomized core in nonlocally coupled oscillators. *Phys. Rev. E*, 69:036213, 2004.
51. J.D. Murray. *Mathematical Biology*. Springer, New York, 1989.
52. B. Ermentrout, J. Campbell, and G. Oster. A model for shell patterns based on neural activity. *Veliger*, 28:369–388, 1986.
53. N.V. Swindale. A model for the formation of ocular dominance stripes. *Proc. R. Soc. London B*, 208:243–264, 1980.
54. D. Tanaka and Y. Kuramoto. Complex Ginzburg-Landau equation with nonlocal coupling. *Phys. Rev. E*, 68:026219, 2003.
55. D. M. Abrams and S. H. Strogatz. Chimera states for coupled oscillators. *Phys. Rev. Lett.*, 93:174102, 2004.
56. D. M. Abrams and S. H. Strogatz. Chimera states in rings of nonlocally coupled oscillators. *Int. J. Bifurcation Chaos*, 16:21–37, 2006.
57. F. M. Atay. Distributed delays facilitate amplitude death of coupled oscillators. *Phys. Rev. Lett.*, 91:094101, 2003.
58. M. Dhamala, V. K. Jirsa, and M. Ding. Enhancement of neural synchrony by time delay. *Phys. Rev. Lett.*, 92:74104, 2004.